minerals

MDPI

Article

An Exploration Study of the Kagenfels and Natzwiller Granites, Northern Vosges Mountains, France: A Combined Approach of Stream Sediment Geochemistry and Automated Mineralogy

Benedikt M. Steiner *, Gavyn K. Rollinson and John M. Condron

Camborne School of Mines, University of Exeter, Penryn Campus, Penryn TR10 9FE, UK; G.K.Rollinson@exeter.ac.uk (G.K.R.); jmc258@exeter.ac.uk (J.M.C.)

* Correspondence: b.steiner@exeter.ac.uk

Received: 1 November 2019; Accepted: 30 November 2019; Published: 3 December 2019

Abstract: Following a regional reconnaissance stream sediment survey that was carried out in the northern Vosges Mountains in 1983, a total of 20 stream sediment samples were collected with the aim of assessing the regional prospectivity for the granite-hosted base and rare metal mineralisation of the northern Vosges magmatic suite near Schirmeck. A particular focus of the investigation was the suspected presence of W, Nb and Ta geochemical occurrences in S-type (Kagenfels) and I-S-type (Natzwiller) granites outlined in public domain data. Multi-element geochemical assays revealed the presence of fault-controlled Sn, W, Nb mineralisation assemblages along the margins of the Natzwiller and Kagenfels granites. Characteristic geochemical fractionation and principal component analysis (PCA) trends along with mineralogical evidence in the form of cassiterite, wolframite, ilmenorutile and columbite phases and muscovite–chlorite–tourmaline hydrothermal alteration association assemblages in stream sediments demonstrate that, in the northern Vosges, S-type and fractionated hybrid I-S-type granites are enriched in incompatible, late-stage magmatic elements. This is attributed to magmatic fractionation and hydrothermal alteration trends and the presence of fluxing elements in late-stage granitic melts. This study shows that the fractionated granite suites in the northern Vosges Mountains contain rare metal mineralisation indicators and therefore represent possible targets for follow-up mineral exploration. The application of automated mineralogy (QEMSCAN®) in regional stream sediment sampling added significant value by linking geochemistry and mineralogy.

Keywords: Vosges; Variscan orogeny; Natzwiller; Kagenfels; granite; lithium; tungsten; niobium; exploration targeting; stream sediments; QEMSCAN®

1. Introduction

Since 2010, the global drive for clean energy and industrial metals led to the delineation and shortlisting of a number of "critical" metals by the European Union [1]. Of the 26 metals listed in the 2017 report, high-tech metals, such as W, Nb and Ta, are of significant importance to the European manufacturing industry. Recent exploration for these metal deposits has been ongoing for more than two decades and has been predominantly focused around known prospective European Variscan belts, such as the Erzgebirge and Cornwall, and characteristic S-type granite provinces therein [2]. A recent regional geochemical reconnaissance sampling campaign, however, identified I-type granites of the lesser known central Vosges Mountains near Sainte-Marie-aux-Mines (France) to be prospective for W and Li-Cs-Ta [3]. Similarly, an investigation of Bureau de Recherches Géologiques

et Minières (BRGM) public domain data [4,5] led to the delineation of a distinct W anomaly in the Natzwiller Granite, which is located in the northern domain of the Vosges Mountains. The northern Vosges Mountains comprise a series of late Devonian–Permian intrusions which show a distinct development from primitive mantle to highly fractionated peraluminous melts and the emplacement of S and I–S-type granites. Detailed studies into the petrology and geochronology of the magmatic suites allowed the reconstruction of a complex magmatic system and evolution of tectonic processes during the Variscan Orogeny [6,7]. The present study aims to investigate the granite-hosted W, Li, Nb and Ta mineralisation potential of the northern Vosges Mountains and provides a link between chemical and mineralogical analyses of regional stream sediment samples and magmatic processes outlined in previous studies. The application of automated mineralogical techniques (QEMSCAN®) to stream sediment samples furthermore aims to demonstrate the usability of this technique in early stage mineral exploration and therefore adds to the limited literature available on the subject [8–10]. Consequently, this paper provides an economic perspective to previous research carried out on the northern Vosges magmatic suite.

2. Geology and Magmatic Pulses of the Northern Vosges Mountains

2.1. Regional Geological Setting

The Vosges Mountains (NE France) are part of the European Variscan orogenic belt and consist of three primary geological domains: the Southern Paleozoic basin (Southern Vosges), the central high grade gneiss and granulite domain (Central Vosges), and the northern low-grade Palaeozoic sedimentary succession (Northern Vosges) [11] (Figure 1a). In this context, the Late Carboniferous Lalaye–Lubine suture, a dextral shear zone, represents the boundary between the Saxothuringian domain of the northern Vosges and the Moldanubian domain of the central and southern Vosges [12]. Throughout the Vosges, a complex suite of Carboniferous magmatic rocks intruded into the early Palaeozoic–Carboniferous basement, predominantly comprising clastic metasedimentary rocks. Over the last three decades, these distinct magmatic suites have instigated significant interest and research into the study of Variscan tectonics and magmatic evolution [13].

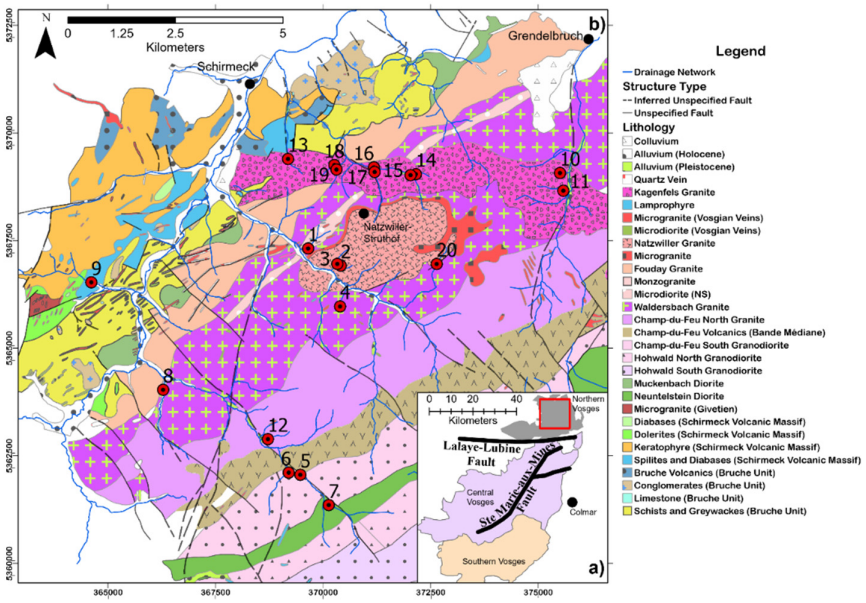

Figure 1. (**a**) Regional geological setting of the Vosges Mountains modified from Tabaud et al. (2015) [12] and (**b**) geological map of the northern Vosges Mountains with focus on the Champ du Feu area, NE France (modified from Bureau de Recherches Géologiques et Minières (BRGM) InfoTerre [4]). Projected coordinate system used: WGS 1984 UTM Zone 32N. Stream sediment sample numbers are indicated as 1–20.

2.2. Magmatic Suites: Geochronology, Geochemistry and Source Rocks

The northern Vosges Mountains (Figure 1b) consist of a Devonian–Carboniferous NE–SW striking succession of (volcano-) sedimentary belts (Bruche Unit, Schirmeck Volcanic "Massif") and weakly metamorphosed sediments of principally clastic origin (Steige Unit, Villé Unit), which were intruded by a Middle Devonian–Permian magmatic suite indicating an overall fractionation trend from tholeiitic to peraluminous S-type melts [6]. The evolution of the magmatic suite is a result of a complex interaction between mantle and crustal source rocks and therefore shows a variety of petrological and geochemical characteristics. The geochronological and geochemical development of these intrusions has been discussed in multiple publications [6,7,14]; however, an overall consensus about the origin and evolution of the granite suites appears to not have been reached yet as other authors question the peraluminous nature of Late Carboniferous granites [15]. In this paper, the geochronological and geochemical framework of the northern Vosges magmatic suites along with the implications for the overall tectonic setting and nature of source rocks will principally be based on the U-Pb zircon age and whole-rock geochemical data provided by Tabaud et al. (2014) [6].

The first magmatic episode took place during the Middle Devonian when continental back-arc tholeiitic to calc-alkaline (sub-aluminous to peraluminous) volcanic rocks of the Schirmeck–Rabodeau massifs were formed as a result of partial melting of a depleted mantle source. These volcanic rocks are generally depleted in Rb and Th. At ca. 330 Ma, calc-alkaline (metaluminous to weakly peraluminous) volcanic rocks of the Hohwald suite (Bande Médiane and Neuntelstein diorites and Hohwald granodiorites) were produced by the partial melting of an enriched mantle wedge followed by fractional crystallisation, crustal assimilation and metasomatism processes. The high-K calc-alkaline Belmont granite suite, comprising the Champ du Feu North, Waldersbach and Fouday granites, was intruded 10 Ma later at ca. 318 ± 3 Ma, and probably formed as a product of the mixing of enriched mantle-derived melt and felsic magma originating from dehydration fluids of subducted continental crust. The "Younger" granite suite, comprising the Andlau, Natzwiller and Senones granite stocks, was intruded at 312 ± 2 Ma and displays typical geochemical properties of felsic Mg-K magmatism, whereas the chemical composition is sub-aluminous to weakly peraluminous. Younger granites are generally enriched in Ba, Sr, Cr, Th, U and ∑REE (Rare Earth Elements). The Younger granites are considered to be derived from the partial melting of an enriched mantle source followed by interaction with subducted, young crustal material and therefore represent a hybrid I-S-type granite. At ca. 290 Ma, in-situ radiogenic heat production resulting from K, Th and U-enriched Younger granites led to crustal anatexis of metasedimentary country rocks and the emplacement of peraluminous to felsic peraluminous S-type Kagenfels granites. Kagenfels two-mica granites are the least ferro-magnesian and the most sodium–potassic rocks of the study area. The rocks are depleted and show negative trends in Ba, Sr, Ti, U and ∑REE, but are enriched in Al, Zr and Hf. The occurrence of metaluminous and peraluminous granites, in the form of the Younger suite and the Kagenfels granite, mirror the overall evolution of the Central Vosges Mg-K (CVMg-K) and Bilstein–Brézouard–Thannenkirch (BBTC) granites of the central Vosges domain. The granite suites in both domains share geochemical similarities and a prominent time lag of 10–15 Ma between the intrusion of I-type CVMg-K (337.2 ± 1.8 Ma) and predominantly S-type BBTC (330–325 Ma) granites [12].

2.3. Mineralisation in the Northern Vosges Mountains and Review of Historic BRGM Regional Geochemical Data

The overall metallogenic setting of the Vosges Mountains has been described in Dekoninck et al. (2017) [16], Fluck and Stein (1992) [17], Fluck (1977) [18] and Fluck and Weil (1976) [19]. Whilst the Central Vosges, in particular, are famous for previously mined post-Variscan polymetallic Pb-Zn-Cu-As-Co-Bi veins along the "Val d'Argent" trend near Sainte-Marie-aux-Mines [20,21], there are limited studies available that explicitly describe the mineralisation patterns of the northern Vosges magmatic suite. Billa et al. (2016) [22] evaluated the regional geochemical trends of historic BRGM data across French basement "massifs". Whilst this report outlined a number of polymetallic and Sn-W anomalies in the southern and central-northern Vosges Mountains, the Belmont Granite Suite of the

northern Vosges around Schirmeck has not been taken into consideration. On the other hand, Weil (1936) [23] noted the presence of adularia, beryl, fluorine and molybdenite in a pegmatite vein ("Grotte des Partisans") located in Kagenfels Granite between Schirmeck, Rothau and Natzwiller. The mineralogical observations confirm the peraluminous nature of S-type Kagenfels Granite and imply that late stage fractionation processes led, locally, to the enrichment of incompatible elements. Leduc (1984) [5] reported results of 905 regional stream sediment samples (data available from BRGM, 2019 [24]) collected across a 330 km^2 extensive area of the northern Vosges Mountains. This survey employed a 125 µm stream sediment fraction along with plasma emission spectroscopy analysis for 22 elements; however, the report does not specify details on the acid leach and analytical precision of the analyses, although these are the only data available for this area. The study resulted in the delineation of a number of polymetallic anomalies in the Fouday, Natzwiller and Kagenfels Granites. For example, distinctive anomalies—i.e., >98th percentile—of W (20–56 ppm) and Sn (27–35 ppm) can clearly be recognised in the eastern parts of the Natzwiller and Kagenfels Granites, respectively (Figure 2a,b, Table 1). Furthermore, elevated concentrations—i.e., >90th percentile—of Nb (41–57 ppm) are present in the Kagenfels Granite and streams draining the Kagenfels area to the north and east (Figure 2c). An analysis of the spatial distribution of Nb is not discussed in Leduc's report. Boron generally shows subdued concentrations of <11 ppm throughout the Natzwiller and Kagenfels Granites, whereas elevated concentrations of 22–63 ppm can be observed in the southeastern margin of the Kagenfels Granite, Ville and Steige schists (Figure 2d).

Table 1. Summary statistics of 579 out of 905 historic BRGM samples located in the study area (Figure 1). The 579 samples were selected from the larger dataset so that the northern Vosges magmatic suite around Hohwald, Champ du Feu, Natzwiller, and imminently adjacent portions of the Bruche Unit and Schirmeck Volcanic Massif, were covered. In total, 22 elements were analysed using Inductively Coupled Plasma Atomic Emission Spectroscopy (ICP-AES); however, only selected available elements of the typical granite-related mineralisation suite are presented here. Note the distinct anomalies of Sn, W (>99th percentile) and Nb (>98th percentile).

Summary Statistics	B (ppm)	Be (ppm)	Cu (ppm)	Nb (ppm)	Sn (ppm)	W (ppm)
Lower Limit of Detection (LoD)	10	1	10	10	20	10
Minimum (LoD/2)	5	0.5	5	5	10	5
Maximum	63	43	155	57	35	56
Mean	10	3.2	17.5	30.3	10.2	5.4
Median	5	3	15	30	10	5
5 percentile	5	0.5	5	16	10	5
10 percentile	5	0.5	5	20	10	5
25 percentile	5	2	5	25	10	5
30 percentile	5	2	11	26	10	5
60 percentile	5	3	16	32	10	5
75 percentile	12	4	21	36	10	5
80 percentile	14	4	23	37	10	5
90 percentile	22	5	31	41	10	5
95 percentile	30	6	42	44	10	5
98 percentile	44	9	63.4	48	10	5
99 percentile	47	22.5	86.4	51.4	27.6	24

Elevated Be concentrations are confined to both the Natzwiller Granite (10–25 ppm) and the Kagenfels Granite (6–43 ppm), highlighting the enrichment of late-stage, incompatible elements in these granites when compared to the surrounding, less-evolved granites of the Belmont Granite Suite (Figure 2e). A prominent Cu anomaly is centred on the Natzwiller Granite (63–136 ppm, Figure 2f). The W, Cu, Nb and Be anomalies are located several hundred meters from the historic Natzwiller–Struthof prison camp quarry which produced "red granite" aggregate during World War II [25]. Whether the metallogenic significance of the Natzwiller and Kagenfels Granites was known to geologists at the time is unclear. Leduc (1984) [5] attributes these anomalies to molybdenite, scheelite, and beryl-bearing pegmatite stringers in Kagenfels Granite, alluvial cassiterite in streams, and chalcopyrite–molybdenite–scheelite (Cu-Mo-W-Ag) veins in Natzwiller Granite, essentially

representing a porphyry mineralisation signature. However, whilst the 22 elements of the analytical suite seemed adequate for the exploration of base metal mineralisation at the time, resistate elements, such as Sn, and also W and Nb, are underestimated by the weak digest and plasma emission technique [5]. Furthermore, the 1980s analytical suite did not contain pathfinder elements (K, Rb, Zr, Hf, Li, Cs, Ta) that are utilised on a routine basis to assess the prospectivity of rare metal granites and pegmatites [26]. For example, K/Rb, Nb/Ta, and Zr/Hf ratios are commonly utilised to support the determination of magmatic fractionation trends, magmatic–hydrothermal interaction during fractional crystallisation, and the enrichment of incompatible elements of possible economic value [27–29]. For this reason, the present investigation aimed to collect a number of independent stream sediment samples in previously identified prospective lithologies, as well as to employ a comprehensive suite of pathfinder elements obtained by Inductively Coupled Plasma Mass Spectroscopy (ICP-MS), along with automated mineralogy techniques, to fingerprint the fractionation and mineralisation processes of the northern Vosges magmatic suite.

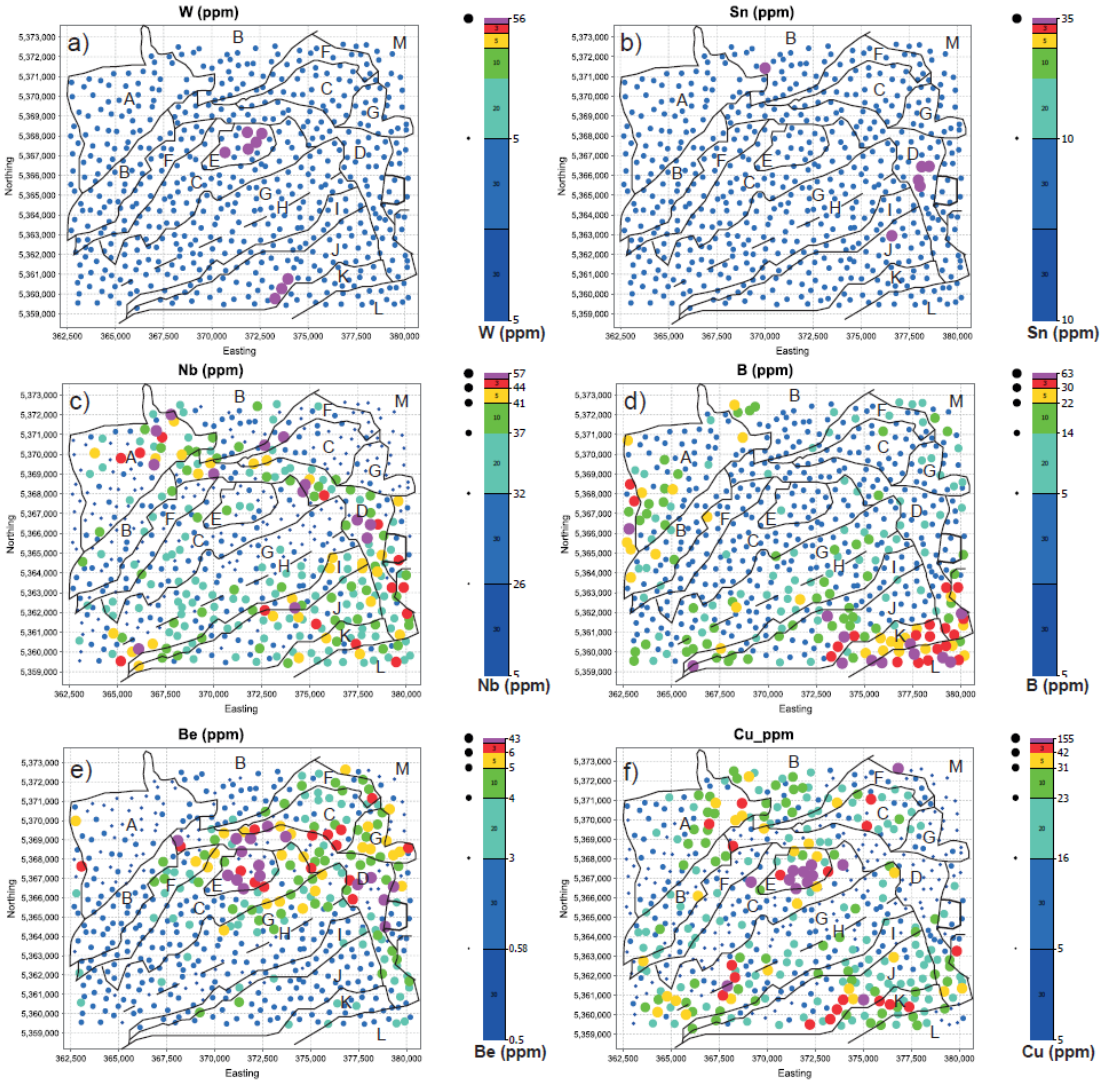

Figure 2. Graduated point symbol maps for (**a**) W, (**b**) Sn, (**c**) Nb, (**d**) B, (**e**) Be, (**f**) Cu using the 30th, 60th, 80th, 90th, 95th, 98th and 99th percentile distribution from Table 1. Principal geological domains are highlighted. A detailed geological map is shown in Figure 1. A, mafic and intermediate volcanic rocks of the Schirmeck Massif; B, metasedimentary rocks of the Bruche Unit; C, Waldersbach Granite; D, Kagenfels Granite; E, Natzwiller Granite; F, Fouday Granite; G, Champ du Feu granite suite; H,

Bande médiane mafic volcanics; I, Neuntelstein Diorite; J, Hohwald granite suite; K, Steige schists; L, Ville schists; M, Lower Buntsandstein.

3. Methodology

In order to obtain an independent dataset and a comprehensive geochemical analysis suite characterised by low detection limits, 20 stream sediment samples (samples 1–20) were collected from first and second-order streams in the Hohwald, Natzwiller, Schirmeck and Grendelbruch areas (Figure 1b). The sample locations were principally designed to test distinctive structural and geochemical trends identified from previous BRGM investigations [5,24] as well as to characterise the different intrusive units across the northern Vosges. The sampling strategy mirrors the workflow and orientation study described in [3]. Samples were collected from stream traps, such as in the lee of large boulders or on point bars, and sieved to retain the <2 mm fraction in the field. The resulting material yielded average weights of 500 g per sample. Samples were stored in plastic bags, zip-tied and labelled with sample ID, coordinates and elevation information. The fine fraction was allowed to settle in the bag before excess water was poured back into the stream. After each sampling location, the equipment was thoroughly cleaned to prevent cross-contamination. A detailed list of stream sample attribute data (colour, grain and mesh size, contamination, trap type, etc.) was recorded on an iPad using ESRI's 'Collector for ArcGIS' app (Version 19.0, ESRI, Redlands, CA, USA). Daily data quality checks and synchronisation with a master database ensured that the data quality was consistent throughout the sampling campaign. Detailed observations and comparisons of drainage sediment composition, outcropping adjacent lithologies and heavy minerals present in pans were noted and supported the lithological classification of samples, along with the identification of fractionated lithologies; for example, quartz or pegmatite-rich rock. Linking observations of stream sediments and adjacent outcrops confirmed that stream sediments appeared unweathered and accurately represent the overall bedrock geology of respective catchment areas, and therefore can be used for further representative lithogeochemical investigations. While glaciation occurred in central–western Europe and affected parts of the central–southern Vosges Mountains, the only glacial debris related to the last glacial event (Weichselian) are recorded in the Bruche River valley. No evidence of glacial sediment was encountered during fieldwork.

Samples were returned to Camborne School of Mines, University of Exeter (UK) laboratories and dried in laboratory ovens at a constant temperature of 40 °C. The samples were then sieved using a sieve stack and a Pascal Sieve Shaker to isolate the <75 μm fraction which was previously identified to be host to W, Li and Cu anomalies in the Vosges [3]. Individual fraction weights were determined to assess if sample loss had occurred. All samples underwent ICP-MS analysis using a standard four acid digest (HCl-HF-HNO_3-$HClO_4$) and Agilent 7700 ICP-MS instrument (Agilent Technologies, Santa Clara, CA, USA), so that, compared to historic studies, a wider range of trace and pathfinder elements, including Nb, Ta, Li, Hf, could be obtained, aiding the determination of fractionation trends (Table 2). Quality control was ensured by inserting silica blanks, duplicate samples and OREAS 147 and 751-certified reference materials into the sample stream, with no accuracy issues noted outside +/− 1 standard deviation of the certified mean value. In a subsequent geochemical interpretation, following a previously published approach in the central Vosges [3] and southeast Ireland [30], the additional ICP-MS assays supported the usage of multi-element major and trace geochemistry in classifying lithological populations and petrogenetic and mineralisation processes. The classification of lithological units was achieved by delineating population clusters in bivariate geochemical plots. Each sample point was assigned a lithology, which was refined using geological observations in upstream catchment areas, outcrops and float in order to better represent subtle nuances in geochemical composition, such as "Natzwiller/Belmont Granite with visible cassiterite".

Of the 20 stream sediment samples (Samples 1–20) undergoing ICP-MS analysis, nine samples (2, 3, 14, 15, 16, 17, 18, 19, 20) of the <75 μm sample fraction were selected for mineralogical analysis. In addition, two rock samples (17A and 18A) were collected within a 10 m distance upstream of their corresponding stream sediment sample locations (17 and 18), and a mineralogical analysis (QEMSCAN®) was performed on uncovered polished thin sections of these samples. Mineralogical

analysis was conducted on the fine <75 um stream sediment fraction, which is considered homogeneous and allowed a direct comparison between mineralogy and geochemistry. The samples were prepared into 30 mm diameter epoxy resin mounts and mixed with pure graphite powder to reduce settling bias and separate particles. The sample surface of the cured mounts was carefully ground to expose the particles and polished to a 1 micron finish using diamond media, then carbon-coated to 25 nm thickness. Samples were analysed using a QEMSCAN® 4300 [31–34] at Camborne School of Mines, University of Exeter, UK. Sample measurement used iMeasure version 4.2SR1 software for data collection and iDiscover 4.2SR1 and 4.3 software for data processing. The Particle Mineral Analysis (PMA) measurement mode was used to map particles at a resolution (pixel spacing) of 2 μm, field size of 600 μm (300 × 300 square, magnification of ×111), default of 1000 X-ray counts per analysis point and a target of 10,000 particles per sample. The final number of particles mapped per sample was higher than this (up to 14,556) due to the system completing the particles in the field it was on when it reached its 10,000-particle target. The number of analysis points per sample varied from 900,000 to 4 million.

The data collected during measurement were processed using a modified version of the standard LCU5 SIP (database), following and building upon details outlined in section 7 of Rollinson et al. (2011) [35]. Both mineral area-% and mineral mass-% (density weighted) data were produced, and it was decided to use the mineral mass-% data as they better reflect the economic mineral content of the samples. As these were stream sediments, the focus was on both the major minerals and trace or unusual minerals, with the SIP customised to reflect the mineralogy of samples. This included checking the mineral identification not just from the measured chemical spectra, but also against in-house mineral reference standards. Moreover, checks were also completed for possible Li minerals following the method developed at Camborne School of Mines during the FAME EU Horizon 2020 project [36]. In the case of identified Ta-Nb minerals, independent SEM-EDS checks were also conducted.

Table 2. Summary statistics of elements and elemental ratios obtained for the present geochemical study. The stream sediment grain size fraction analysed was <75 μm. All 20 samples were analysed by ICP-MS using a four-acid digest (HCl-HF-HNO_3-$HClO_4$).

	As (ppm)	B (ppm)	Be (ppm)	Cs (ppm)	Cu (ppm)	Hf (ppm)	K (ppm)	Li (ppm)	Nb (ppm)	Pb (ppm)	Rb (ppm)
Lower Limit of Detection	0.0003	4.14	0.0003	0.0007	0.00005	0.0003	0.006	0.0002	0.0003	0.0003	0.0003
Minimum	7.28	9.9	1.25	3.59	7.88	8.65	12,513	12.13	9.93	8.72	47.3
Maximum	125.97	60.25	34.22	27.42	375.63	64.86	25,376	105.1	198.29	99.56	366.6
Mean	40.13	16.11	10.73	12.62	96	29.45	18,210	53.51	67.41	43.94	140.69
Median	27.1	14.08	10.21	11.93	77.71	30.51	18,226	50.57	58.41	39.39	136.4
5 percentile	7.37	9.9	1.27	3.79	8.74	8.7	12,533	12.83	10.11	9.29	67.1
10 percentile	9.07	9.97	1.79	7.78	26.84	9.66	13,087	26.96	13.59	20.73	77.9
25 percentile	15.62	12.04	2.8	9.79	50.18	14.4	15,382	41.4	16.03	27.3	112.75
30 percentile	16.75	12.28	3.08	10.56	54.09	17.73	15,536	41.65	19.06	29.79	116.3
60 percentile	38.63	15.06	11.82	12.08	87.94	35.13	19,110	53.9	82.25	40.44	144.9
75 percentile	64.57	15.43	13.61	14.13	119.21	39.51	20,371	66.09	97.96	53.73	162.55
80 percentile	72.9	15.45	18.08	16.08	122.23	44.12	21,099	75.96	100.08	54.28	175.2
90 percentile	91.78	21.34	23.83	19.37	175.49	50.68	23,542	81.37	185.66	92.04	192.5
95 percentile	124.31	58.34	33.71	27.03	365.67	64.15	25,289	103.92	197.99	99.27	215.7
98 percentile	125.97	60.25	34.22	27.42	375.63	64.86	25,376	105.1	198.29	99.56	316.76
99 percentile	125.97	60.25	34.22	27.42	375.63	64.86	25,376	105.1	198.29	99.56	366.6

	Sn (ppm)	Sr (ppm)	Ta (ppm)	Th (ppm)	Ti (ppm)	W (ppm)	Zr (ppm)	K/Rb	Nb/Ta	Zr/Hf
Lower Limit of Detection	0.0003	0.0003	0.0003	0.0003	0.0007	0.0006	0.0003			
Minimum	5.48	21.41	0.76	8.87	2171	1.8	346.08	64.5	8.03	19.13
Maximum	41.55	291.31	11.77	93.73	10,503	102.56	1923.08	273.2	17.75	45.01
Mean	18.89	132.38	4.55	41.5	4676	21.84	962.67	134.74	13.41	34.75
Median	18.39	133.64	3.93	39.7	4171	13.2	857.43	131	12.88	36.93
5 percentile	5.52	22.15	0.78	8.93	2194	1.8	347.69	100.25	8.04	19.43
10 percentile	6.33	36.91	1.183	10.1	2652	2.05	378.59	104.2	8.52	25.26
25 percentile	10.87	59.5	1.83	16.82	3721	7.4	588.84	111	11.19	27.48
30 percentile	13.39	84.617	1.87	20.21	3857	9.26	702.17	102.38	11.67	31.07
60 percentile	19.82	144.036	5.12	47.2	4531	21.8	902.79	125	13.99	38.3
75 percentile	25.2	182.54	7.06	64.56	5386	29.01	1368.48	141.2	16.641	40.01
80 percentile	29.81	196.41	7.53	66.27	5531	33.67	1434.81	146.76	16.82	41.03
90 percentile	33.74	257.58	10.56	85.67	8344	48.52	1819.55	228.35	16.87	42.57
95 percentile	41.18	289.86	11.72	93.37	10,410	99.92	1918.6	271.4	17.71	44.89
98 percentile	41.55	291.31	11.77	93.73	10,503	102.56	1923.08	273.2	17.75	45.01
99 percentile	41.55	291.31	11.77	93.73	10,503	102.56	1923.08	273.2	17.75	45.01

4. Results

4.1. Univariate Anomaly Analysis of Ore and Incompatible Elements

Graduated point symbol maps of incompatible elements (Figure 3) show an overall enrichment above the 95th percentile of W (99.92 ppm), Nb (197.99 ppm), Ta (11.72 ppm) and Be (33.71 ppm) in Kagenfels Granite. Compared to average concentrations of W (2 ppm), Nb (20 ppm), Ta (3.5 ppm) and Be (5 ppm) in granites [37], the Kagenfels Granite is locally characterised by an enrichment factor of more than 50 (W), 10 (Nb), 3.4 (Ta) and 6.7 (Be). The anomalous samples are located approximately 600–900 m north of the Natzwiller–Struthof camp at confluences with the Barembach stream (samples 13–19, Figure 1b) as well as the Magel stream to the east (samples 10–11). The anomalous zones principally correlate with regional NNE–SSW trending fault zones, where this study additionally located occurrences of 2–3 m wide, partially overburden-covered quartz–feldspar pegmatitic granite stringers trending parallel to these fault zones, particularly at sample location 18. In addition, the Kagenfels Granite is characterized by distinct magmatic fractionation ratios of $64.5 < K/Rb < 110$, $13.98 < Nb/Ta < 17.75$ and $19.12 < Zr/Hf < 37.91$. On the other hand, the southwestern part of the Natzwiller Granite displays an enrichment of Li (105.1 ppm), W (34.81 ppm) and B (21.99 ppm) corresponding to enrichment factors of 3.5 (Li), 17.4 (W) and 1.5 (B), respectively. Fractionation ratios of $101 < K/Rb < 128.8$, $12.35 < Nb/Ta < 12.7$, $33.85 < Zr/Hf < 36.45$ are slightly more elevated than the Kagenfels Granite, indicating generally less fractionation. Sample 20, located on a fault-controlled boundary between the Natzwiller Granite and Belmont Granite Suite, shows visible cassiterite in a stream pan, but only limited concentrations of Sn (17.98 ppm) and the highest K/Rb (273.2) ratio of the sampling campaign. The presence of coarse cassiterite visible in a pan and limited concentrations of Sn in the < 75 um fraction suggest a strong partitioning of Sn by size fraction. Cassiterite was not abraded and comminuted to finer size fractions due to the limited fluvial transport and therefore is thought to originate from a proximal source. The Belmont Granite Suite, comprising the Fouday, Waldersbach, Champ du Feu North Granites along with three samples collected in the older Neuntelstein Diorite and Hohwald Granodiorites, is typically characterised by an absence of notable concentrations of incompatible elements, whereby fractionation ratios of $113.5 < K/Rb < 237.1$, $37.42 < Zr/Hf < 45$ imply a less fractionated nature than the Natzwiller and Kagenfels Granites. The calculated Nb/Ta ratio of 8–13.1, however, is considerably lower than the Natzwiller and Kagenfels Granites.

4.2. Geochemical Classification of Principal Rock Units and Magmatic Fractionation Using Stream Sediment Data

The analysis of trace element concentrations, supported by geological observations in outcrops and stream catchment areas, led to the classification of four major regional lithology types (Figure 4). Stream sediment geochemistry was classified per lithology unit, and the link between the stream sediment geochemistry and lithology was investigated. The lithologies principally reflect the regional BRGM geological map of the northern Vosges Mountains. Major and trace elements and ratios used in this study are predominantly Ti, Th, B, K/Rb, Nb/Ta, and Zr/Hf. A combination of these elements supports the determination of significant petrological and fractionation processes characteristic for each lithology of the northern Vosges magmatic suite.

Kagenfels Granite was macroscopically distinguished in outcrop and stream sediments from other lithologies by the presence of muscovite, biotite, ilmenite, and minor beryl. The lithology forms distinct population clusters in Ti vs. Th, K/Rb vs. Th and Ti vs. B bivariate plots with concentrations of Th (38.33–86.53 ppm), Ti (2170–5683 ppm), B (9.9–13.85 ppm), $64.5 < K/Rb < 110$, and $19.12 < Zr/Hf < 37.91$. Whilst the K/Rb and Zr/Hf ratio of samples 10–11, 13–14, and 18 represent the lowest, and therefore most fractionated, magmatic fractionation indicator values in the studied samples, Nb/Ta ratios of 13.98–17.75 are unexpectedly high.

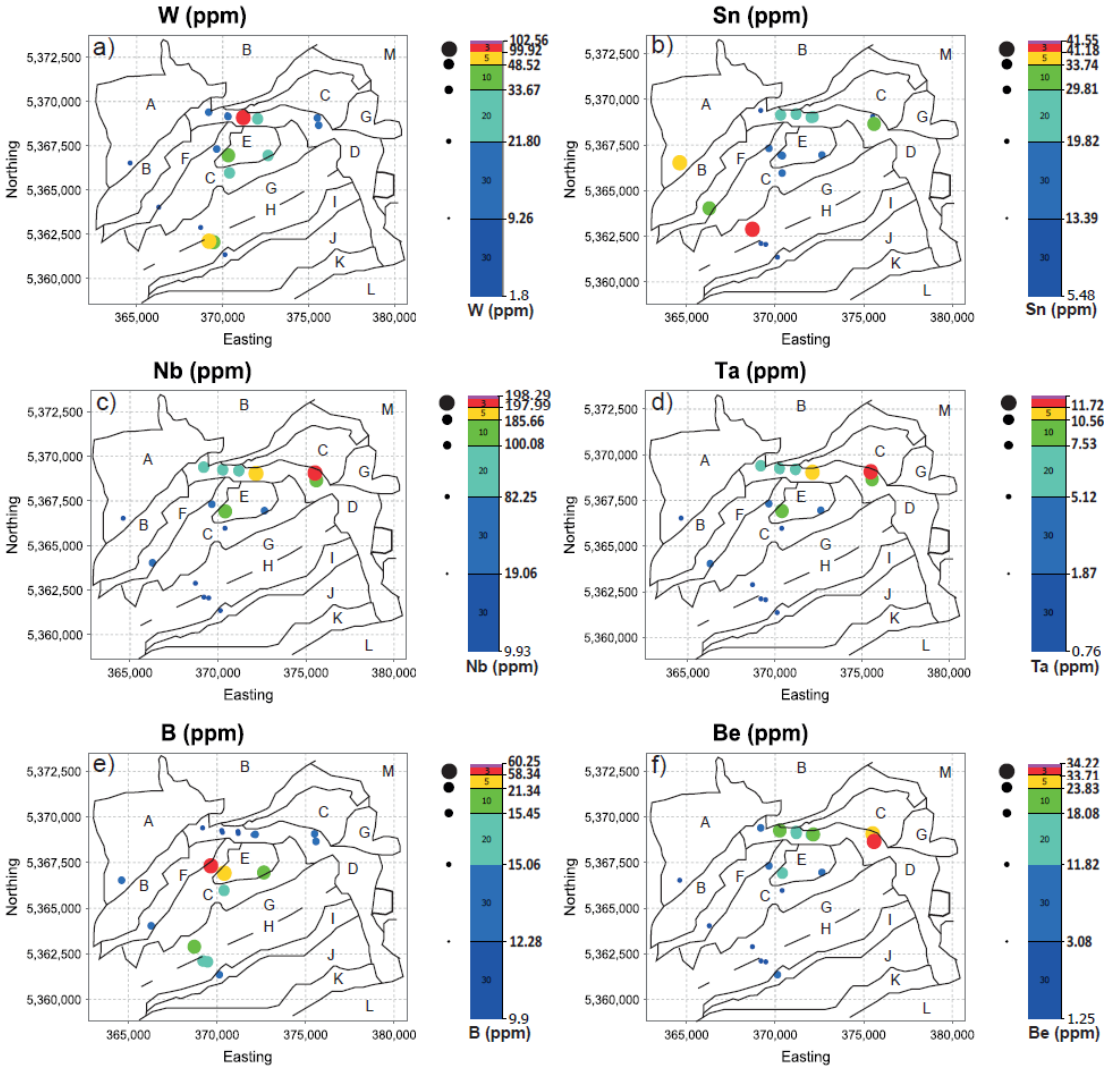
W (ppm)
a)
Sn (ppm)
b)
Nb (ppm)
c)
Ta (ppm)
d)
B (ppm)
e)
Be (ppm)
f)
Northing
Easting
5,372,500
5,370,000
5,367,500
5,365,000
5,362,500
5,360,000
365,000
370,000
375,000
380,000
A
B
C
D
E
F
G
H
I
J
K
L
M
102.56
99.92
48.52
33.67
21.80
9.26
1.8
W (ppm)
41.55
41.18
33.74
29.81
19.82
13.39
5.48
Sn (ppm)
198.29
197.99
185.66
100.08
82.25
19.06
9.93
Nb (ppm)
11.72
10.56
7.53
5.12
1.87
0.76
Ta (ppm)
60.25
58.34
21.34
15.45
15.06
12.28
9.9
B (ppm)
34.22
33.71
23.83
18.08
11.82
3.08
1.25
Be (ppm)

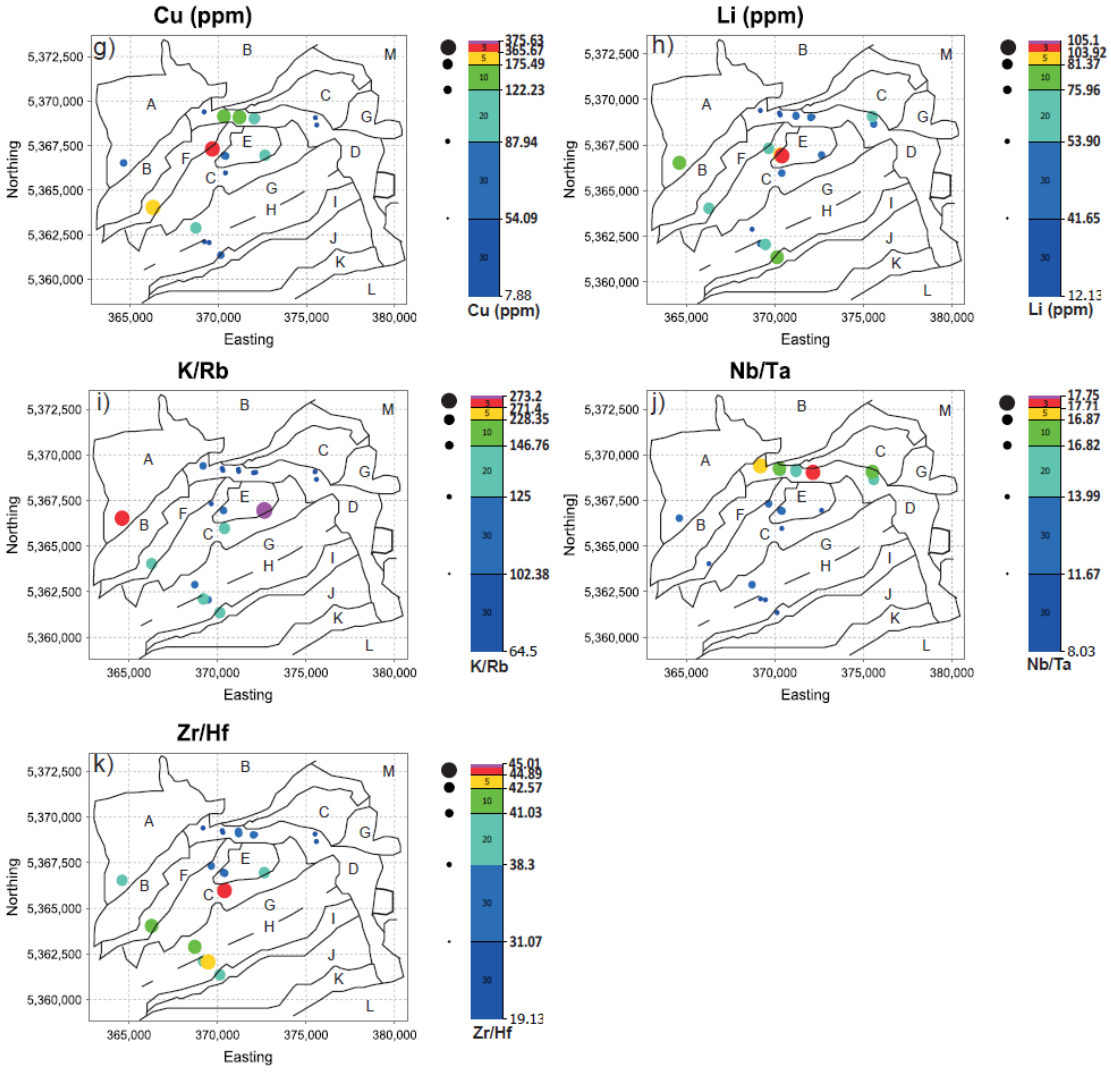

Figure 3. Graduated point symbol maps for (**a**) W, (**b**) Sn, (**c**) Nb, (**d**) Ta, (**e**) B, (**f**) Be, using the 30th, 60th, 80th, 90th, 95th, 98th and 99th percentile distribution from Table 1. Principal geological domains are highlighted in panel (**a**). A, mafic and intermediate volcanic rocks of the Schirmeck Massif; B, metasedimentary rocks of the Bruche Unit; C, Waldersbach Granite; D, Kagenfels Granite; E, Natzwiller Granite; F, Fouday Granite; G, Champ du Feu granite suite; H, Bande médiane mafic volcanics; I, Neuntelstein Diorite; J, Hohwald granite suite; K, Steige schists; L, Ville schists; M, Lower Buntsandstein. Graduated point symbol maps for (**g**) Cu, (**h**) Li, (**i**) K/Rb, (**j**) Nb/Ta and (**k**) Zr/Hf.

Natzwiller Granite contains macroscopic evidence of biotite, amphibole, hematite, ilmenite and rutile and is generally darker in appearance. This population can be geochemically distinguished from Kagenfels Granite and forms two distinct clusters in Ti vs. Th and Ti vs. B bivariate plots, with higher concentrations of Ti (8639–10,502 ppm), Th (77.95–93.73 ppm), and B (15.41–21.99 ppm). The K/Rb ratio varies from 101–128.8; i.e., it is reasonably similar to the Kagenfels Granite. The abundant visual presence of rutile, ilmenite, and magnetite in the stream sediment and outcrop supports the elevated contents of Ti, implying a more intermediate composition than the Kagenfels Granite. Natzwiller Granite plots on the southern and eastern margins of the corresponding BRGM lithology (Figure 1). Sample 20 contained abundant panned cassiterite which occurs along the faulted contact between the Natzwiller and Waldersbach granites. The sample was classified as Natzwiller/Belmont Granite with visible cassiterite. This K-feldspar and quartz-rich stream sediment sample has the highest K/Rb value of 273.2 and is generally depleted of trace elements.

The Belmont Granite Suite comprising the Fouday, Champ du Feu and Waldersbach granites [6,7] forms a distinct population cluster in Ti vs. Th, Ti vs. B, and K/Rb vs. Th bivariate plots, and can be clearly distinguished from the Kagenfels and Natzwiller granites by lower concentrations of the aforementioned elements, particularly Th (8.87–24.45 ppm), and has K/Rb and Zr/Hf values ranging from 105–165 and 37.42–45, respectively. The Hohwald Granodiorite (samples 5–6) and the Neuntelstein Diorite (sample 7) plot within this lithogeochemical population have therefore been included in the present Belmont Granite suite classification.

A principal component analysis (PCA) of the geochemical dataset was carried out using a log10 transformation (to eliminate the closure effect) of B, Be, Cu, Li, Nb, Rb, Sn, Ta, Th, Ti, W and Zr input variables (Table 3, Figure 5). The PCA revealed that PC1 to PC4 represent 85.68% of the total variance of the dataset, whereas the remaining eight PCs can be attributed to random processes or noise. The eigenvector table and combined variable-sample analysis (RQ) plots, in which samples plot as points and variables as vectors with the length of the vectors proportional to the variability of the two displayed principal components, outline two major correlations and elemental trends. Firstly, previously classified Kagenfels and Natzwiller Granites are principally characterised by negative RQ1 loadings, whereas Natzwiller Granite can be distinguished from Kagenfels Granite by positive RQ2 and RQ4 loadings. On the other hand, there is a noteworthy variability of the Kagenfels Granite samples 10–11, 13–14 and 18, expressed by generally negative RQ2 and RQ4 loadings of Rb and Zr, respectively. In the K/Rb vs. Zr/Hf plot (Figure 4e), these samples represent the most fractionated population with K/Rb < 120 and Zr/Hf < 32. Therefore, the PCA trends are distinctive for the previously outlined fractionated lithogeochemical populations and characterised by a Ta-Nb-Be-Rb-Th-W and Zr geochemical association. In particular, whilst PC1 broadly characterises fractionated lithologies of the Kagenfels and Natzwiller Granites in the study area, PC2 and PC4 allow the determination of local variation of fractionation in the Kagenfels Granite. In contrast, the Belmont Granite Suite and the Natzwiller/Belmont Granite with visible cassiterite (sample 20) show fundamentally different trends with positive RQ1 loadings, and a Cu-Ti and Li geochemical association. Distinctive negative and positive variability in RQ2 and RQ4, respectively, allow the determination of potential sub-populations, such as samples 6 (Hohwald Granodiorite) and 7 (Neuntelstein Diorite), which are generally less evolved and have intruded approximately 10 Ma earlier than the Belmont Suite [6]. In summary, the analysis of petrogenetic indicator elements in bivariate plots along with principal component analysis provide a robust tool to determine different litho-geochemical populations and element associations in the study area.

4.3. Bulk Mineralogy, Indicators for Magmatic Fractionation and Link to Stream Sediment Geochemistry

4.3.1. Correlation between Outcrop and Stream Sediment Sample Mineralogy

In order to ascertain the representativity of stream sediment samples and previously mapped lithological units, a comparison between the modal mineralogy of stream sediment and adjacent outcrop samples has been undertaken. Stream sediment samples 17 and 18 are located in the northern part of the Kagenfels Granite unit and are enriched in W (102.56 ppm and 6.94 ppm) and Nb (63.67 ppm and 92.76 ppm), respectively. Visual field mapping and description of drainage areas and sediments confirm the presence of a muscovite–biotite(–tourmaline) granite, along with sporadically occurring pods of a finer, hornblende-bearing variety, which was previously described as the less evolved "rhyolite facies" of the Kagenfels Granite [14]. Abundant outcrops of the granite are present several hundred metres upstream of the sampled locations, whilst pods of the "rhyolite facies" are encountered in the vicinity of the stream sources along the margins of the granite. Sample 18 yielded minor columbite grains during routine pan inspection. The QEMSCAN modal mineralogy of stream sediment samples 17 and 18 (Table 4) confirms the peraluminous monzogranitic nature of the samples containing tourmaline (1.43%, 0.82%), muscovite (1.34% and 1.37%), and spessartine (0.14% and 0.65%) as abundant accessory Al-rich mineral phases. Furthermore, wolframite (0.03% in 2060) and ilmenorutile (0.01% and 0.05%) represent the hosts for W and Nb-rich accessory mineral phases, which correlate with the geochemical anomalies outlined in this study.

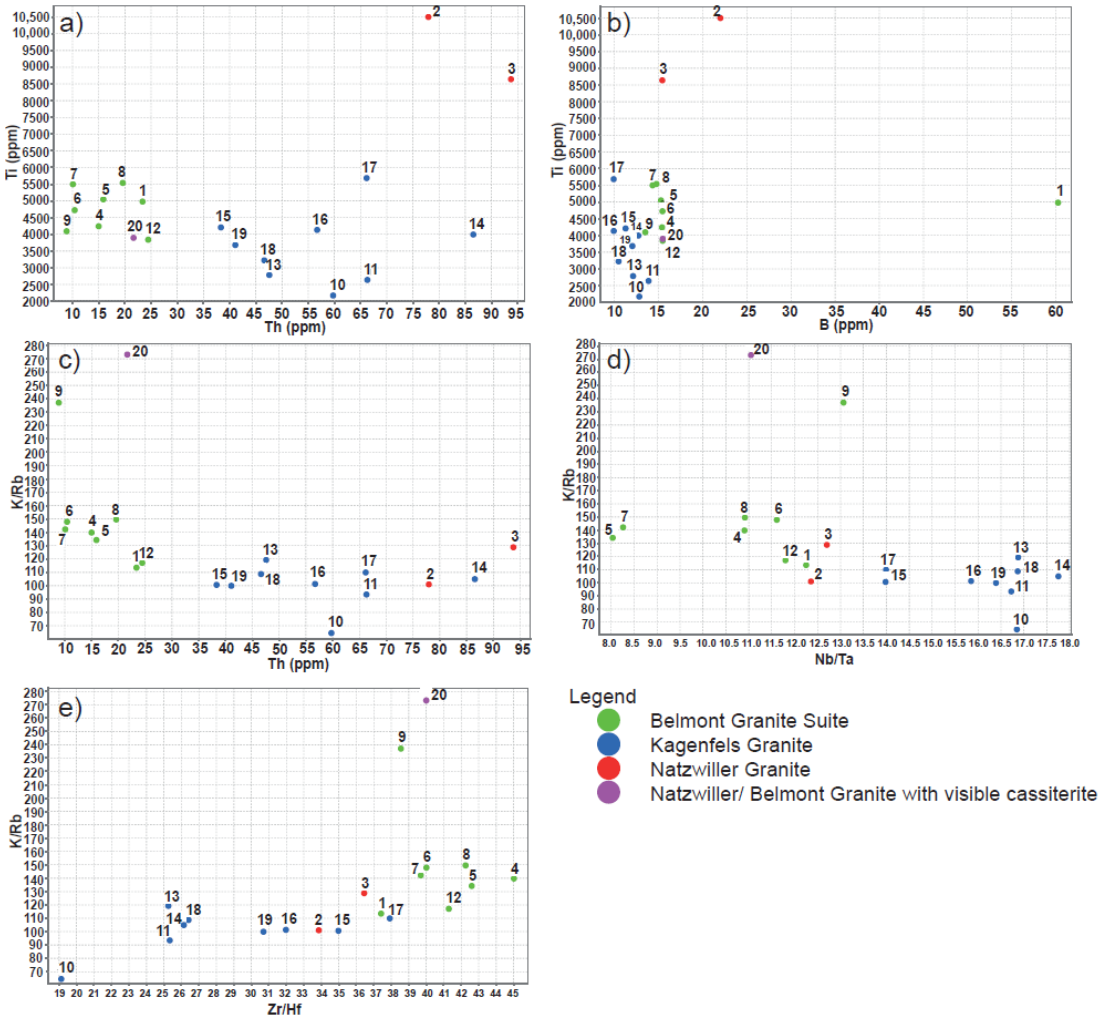

Figure 4. Binary plots of stream sediment geochemistry represented by broad lithological units in the drainage basin. (**a**) Ti vs. Th, (**b**) Ti vs. B, (**c**) K/Rb vs. Th, (**d**) Nb/Ta, and (**e**) Zr/Hf. Sample identification numbers are plotted in the graphs. Each population displays a characteristic clustering trace element assemblage. The stream sediment samples obtained downstream of the Belmont Granite suite generally has a less fractionated nature than the Natzwiller and Kagenfels Granites expressed in comparatively higher K/Rb and Zr/Hf ratios and lower Th concentrations. Decreasing fractionation indices (K/Rb, Nb/Ta and Zr/Hf) indicate an increasing influence of magmatic–hydrothermal interactions during fractional crystallization [27]. Stream sediment sample numbers are indicated as 1–20.

Table 3. Principal component analysis of the stream sediment geochemical dataset showing (a) correlation of elements, (b) eigenvalues, and (c) scaled coordinates. Grey colours display an average correlation range (0.5–0.7), light brown a good correlation range (0.7–0.9) and purple a very good correlation range (0.9–1)

(a) Correlation	B (ppm)	Be (ppm)	Cu (ppm)	Li (ppm)	Nb (ppm)	Rb (ppm)	Sn (ppm)	Ta (ppm)	Th (ppm)	Ti (ppm)	W (ppm)	Zr (ppm)
B (ppm)	1	−0.22	0.43	0.38	−0.23	−0.26	0.07	−0.19	−0.2	0.32	−0.1	−0.45
Be (ppm)	−0.22	1	−0.11	−0.26	0.93	0.75	−0.04	0.93	0.87	−0.28	0.17	0.57
Cu (ppm)	0.43	−0.11	1	0.49	−0.23	−0.36	0.52	−0.21	−0.08	0.44	−0.02	−0.02
Li (ppm)	0.38	−0.26	0.49	1	−0.32	−0.23	0.19	−0.22	−0.2	0.64	0	-0.1
Nb (ppm)	−0.23	0.93	−0.23	−0.32	1	0.81	−0.1	0.98	0.94	−0.23	0.21	0.62
Rb (ppm)	−0.26	0.75	−0.36	−0.23	0.81	1	−0.01	0.77	0.67	−0.55	0.02	0.35
Sn (ppm)	0.07	−0.04	0.52	0.19	−0.1	−0.01	1	−0.15	0.07	0.08	−0.19	0.21
Ta (ppm)	−0.19	0.93	−0.21	−0.22	0.98	0.77	−0.15	1	0.94	−0.13	0.24	0.63
Th (ppm)	−0.2	0.87	−0.08	−0.2	0.94	0.67	0.07	0.94	1	0	0.31	0.77
Ti (ppm)	0.32	−0.28	0.44	0.64	−0.23	−0.55	0.08	−0.13	0	1	0.26	0.21
W (ppm)	−0.1	0.17	−0.02	0	0.21	0.02	−0.19	0.24	0.31	0.26	1	0.51
Zr (ppm)	−0.45	0.57	−0.02	−0.1	0.62	0.35	0.21	0.63	0.77	0.21	0.51	1

(b)	Eigenvalues	Percent	Cumulative %
PC1	5.321	44.35	44.35
PC2	2.386	19.88	64.23
PC3	1.432	11.93	76.16
PC4	1.143	9.524	85.68
PC5	0.6511	5.426	91.11
PC6	0.5012	4.177	95.28
PC7	0.3569	2.974	98.26
PC8	0.09674	0.8062	99.06
PC9	0.07267	0.6056	99.67
PC10	0.02147	0.1789	99.85
PC11	0.0125	0.1042	99.95
PC12	0.005843	0.04869	100

(c) Scaled Coordinates	PC1	PC2	PC3	PC4	PC5	PC6	PC7	PC8	PC9	PC10	PC11	PC12
B (ppm)	0.408	0.3572	0.3255	0.6315	0.3509	0.01225	0.2645	0.04051	0.07987	0.00297	0.00218	0.00289
Be (ppm)	−0.917	0.1213	0.1951	0.1241	0.04045	−0.04277	−0.1874	0.2209	−0.03386	−0.02367	0.04212	−0.00409
Cu (ppm)	0.3415	0.72	0.3555	−0.09954	0.2485	−0.03138	−0.3918	−0.1048	0.03856	−0.00284	0.00383	−0.00283
Li (ppm)	0.4033	0.6475	0.07263	0.2348	−0.4995	0.3126	−0.06785	0.06441	0.00516	0.0317	−0.02365	0.00966
Nb (ppm)	−0.9695	0.09748	0.1066	0.1512	0.01134	−0.0767	−0.00449	−0.05642	−0.04153	−0.03102	−0.0283	0.05989
Rb (ppm)	−0.8252	−0.1733	0.3217	0.1054	−0.1527	0.3506	0.06946	−0.1358	0.03502	−0.03331	0.05013	−0.01149
Sn (ppm)	0.1	0.4327	0.5633	−0.6311	0.0861	0.1112	0.2403	0.0451	−0.0835	−0.01961	−0.01414	−0.00206
Ta (ppm)	−0.9489	0.1672	0.05228	0.2242	−0.04822	−0.09056	−0.00587	−0.02147	−0.00787	−0.03192	−0.0687	−0.04341
Th (ppm)	−0.917	0.3374	0.04044	0.02026	0.02975	−0.1245	0.08018	−0.05258	−0.06128	0.1162	0.01846	−0.00596
Ti (ppm)	0.316	0.7821	−0.3607	0.1243	−0.2014	−0.2717	0.1259	−0.05419	−0.07271	−0.05353	0.03931	−0.00605

W (ppm)	−0.2828	0.3478	−0.7064	−0.00598	0.371	0.3977	−0.01112	0.007	−0.0623	−0.00659	−0.00518	−0.00106
Zr (ppm)	−0.6948	0.4521	−0.3004	−0.4066	−0.05321	−0.06105	0.09301	0.03585	0.2018	−0.00142	0.00119	0.00592

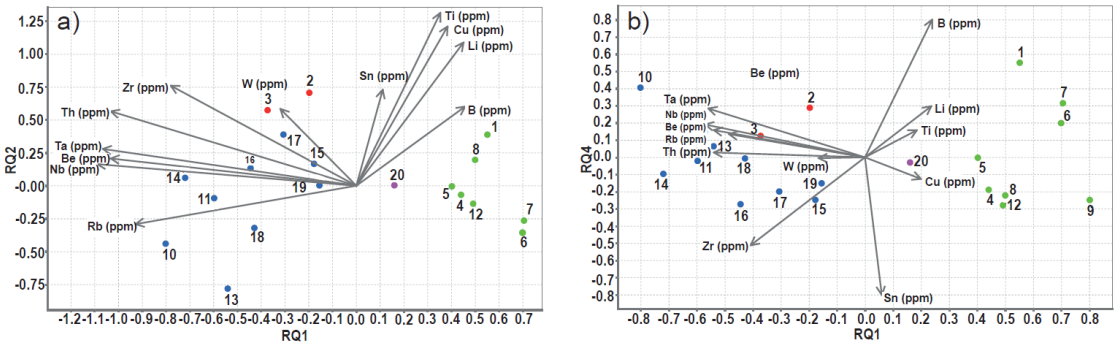

Figure 5. Principal component analysis of the stream sediment geochemical dataset showing (**a**) RQ1–RQ2 plot and (**b**) RQ1–RQ4 plots. In combined variable-sample analysis (RQ) plots, samples plot as points and variables as vectors, with the length of the vectors proportional to the variability of the two displayed principal components. The legend is as seen in Figure 4. The data clearly demonstrate that the Kagenfels and Natzwiller Granite are characterised by negative RQ1 loadings, whilst the Belmont Granite Suite has fundamentally positive RQ1 loadings. Natzwiller Granite can be distinguished by positive RQ1 and RQ4 loadings. The local fractionation of Kagenfels Granite is obvious from variable RQ2 and RQ4. Stream sediment sample numbers are indicated as 1–20.

The mineralogical analysis of the collected samples confirms that major silicate phases (e.g., quartz, feldspars, micas, and tourmaline) of the −75 µm fraction are not or very weakly weathered and generally do not show weathering rims or the complete replacement of the mineral grains with kaolinite (Figure 6). This implies a rapid erosion of outcrops and (re)deposition in stream traps. Variable amounts of Fe-Mn oxides are present in the samples and indicate that the weathering of primary Fe-rich minerals can to some extent affect stream sediments of the study area.

The outcropping muscovite–biotite(–tourmaline) host granite bedrock samples 17B and 18B display a comparable monzogranitic composition and variably contain more abundant K-Feldspar (10–14%) and quartz (5–10%) than the stream sediments. Importantly, both rock samples are characterised by similar, yet slightly subdued, amounts of key accessory minerals, such as tourmaline (0.29% and 0.22%), muscovite (0.46% and 0.42%), ilmenite (0.09% and 0.18%) and rutile (0.04%). Due to local variations in bedrock geology and the nature of sample origin and preparation techniques (i.e., a thin section of a singular outcrop chip vs. well-mixed stream sediment samples), trace and heavy minerals will naturally be more abundant in samples obtained from stream traps where the accumulation of denser mineral grains is more pronounced. Conversely, minerals with a lower specific gravity, such as quartz, mica and feldspar, will likely be less abundant in stream sediments than in outcrop. The mineralogical analysis of stream sediments and outcropping bedrock, however, demonstrates that the mineralogical composition of stream sediments is generally indicative of its corresponding source lithology. As a result, it can be assumed that the largely unweathered stream sediment samples reflect the overall lithological composition and are representative of the stream catchments.

4.3.2. Petrogenetic Indicators

Other samples obtained and analysed from the Kagenfels Granite (Appendix A) show similar modal mineralogical compositions compared to stream sediment samples 17 and 18 and therefore provide evidence for peraluminous two-mica monzogranite. In particular, stream sediment samples 14–16, 19 and 20 are characterised by the presence of muscovite (0.80–1.97%), biotite (1.26–2.01%), tourmaline (0.51–1.43%), chlorite (1.47–3.52%), ilmenite (0.28–0.98%), ilmenorutile (0.01–0.05%), zircon (0.54–3.1%), monazite (0.01–0.4%), cassiterite (0.01% in sample 16) and columbite (0.01%). Ilmenorutile is commonly intergrown with rutile and ilmenite (Figure 7) and columbite can be found as inclusions in cassiterite (Figure 8). Further follow-up by SEM confirmed the presence of various Nb-rich phases (Mn-columbite, U-rich euxenite-(Y), and Nb-rich titanium oxide/ ilmenorutile) in

sample 17 (Figure 9), which, together with a high geochemical Nb/Ta ratio of 14, implies that Nb-rich mineral phases are distinctively more abundant than Ta phases in the western part of the Kagenfels Granite. Sample 18 (Figure 10) shows that chlorite is associated with tourmaline and muscovite and therefore represents evidence for granite-related magmatic–hydrothermal alteration [38]. However, due to the size of the fragments and the absence of quartz, it is not entirely conclusive whether this mineral association is related to veins or wall-rock alteration.

Stream sediment samples 2 and 3, obtained from the two principal drainages on the southwestern flank of the Natzwiller Granite, generally show a similar monzogranitic composition as the Kagenfels Granite. Accessory Th- and Ti-bearing mineral phases in Natzwiller and Kagenfels Granites (Table 4) indicate a comparable content of Th-rich mineral phases, with the highest content (1.91 mass-%) of Ti-phases in sample 3. This generally corresponds to the Th vs. Ti bivariate plot (Figure 5a), where the Natzwiller Granite samples have Ti concentrations of >8640 ppm. However, given the notable enrichment of Ti in the geochemical analyses, a higher abundance of Ti mineral phases would be expected in the mineralogical analysis. However, this may be explained by the occurrence of trace Ti occurring in other minerals, such as micas [39]. A distinctive feature of samples 2 and 3, on the other hand, is the abundance of tourmaline (8.48% and 3.39%) and chlorite (13.61% and 6.88%), which in Figure 5b correspond to a distinctive B signature of 21.99 ppm and 15.41 ppm, respectively, and associated Nb (100.33 ppm and 94.64 ppm), Ta (8.12 ppm and 7.45 ppm), Nb/Ta (12.35 and 12.7) and W (21.55 ppm and 34.81 ppm).

Table 4. Modal mineralogy (mineral mass-%) of selected stream sediment and outcrop samples of the Kagenfels (17A and 18B) and Natzwiller Granites (2 and 3). The four stream sediment samples show a broadly similar monzogranitic composition; however, the Natzwiller Granite has generally more abundant B and Ti-rich mineral phases—e.g., tourmaline and rutile. Outcropping rocks and stream sediments of the Kagenfels granite have a comparable mineralogical composition; however, with a subdued heavy mineral signature. Please refer to Appendix 1 for a complete list of sample mineralogy tables.

Stream Sediment 2		Stream Sediment 3		Stream Sediment 17		Stream Sediment 18		Rock 17A		Rock 18A	
Plagioclase	27.08	Plagioclase	29.01	Plagioclase	29.24	Plagioclase	36.97	K-Feldspar	35.78	Quartz	36.55
Quartz	19.6	K-Feldspar	20.96	Quartz	24.10	K-Feldspar	25.9	Plagioclase	32.23	K-Feldspar	31.35
K-Feldspar	18.53	Quartz	19.65	K-Feldspar	22.14	Quartz	24.34	Quartz	29.44	Plagioclase	29.65
Chlorite	13.61	Chlorite	6.88	Fe-Ox (Mn)/CO3	5.89	Chlorite	2.56	Fe-Ox (Mn)/CO3	0.77	Fe-Ox (Mn)/CO3	0.8
Tourmaline	8.48	Fe-Ox (Mn)/CO3	6.73	Chlorite	3.52	Fe-Ox (Mn)/CO3	1.91	Biotite	0.72	Biotite	0.53
Biotite	3.26	Hornblende	3.86	Zircon	3.10	Biotite	1.79	Muscovite	0.46	Muscovite	0.42
Fe-Ox (Mn)/CO3	2.07	Tourmaline	3.39	Hornblende	3.03	Muscovite	1.37	Tourmaline	0.29	Tourmaline	0.22
Hornblende	1.92	Zircon	2.3	Biotite	2.01	Ilmenite	0.91	Chlorite	0.12	Ilmenite	0.18
Muscovite	1.12	Biotite	1.98	Tourmaline	1.43	Tourmaline	0.82	Ilmenite	0.09	Chlorite	0.12
Rutile	1.09	Apatite	1.26	Muscovite	1.34	Spessartine	0.65	Rutile	0.04	Kaolinite	0.05
Kaolinite	0.76	Rutile	1.11	Apatite	0.97	Zircon	0.56	Zircon	0.02	Rutile	0.04
Zircon	0.57	Muscovite	0.71	Rutile	0.70	Hornblende	0.48	Ti-Magnetite	0.01	Zircon	0.03
Ca-Fe-Al silicates	0.38	Ca-Fe-Al silicates	0.42	Ilmenite	0.60	Rutile	0.41	Monazite	0.01	Ti-Magnetite	0.02
Titanite	0.17	Titanite	0.37	Ca-Fe-Al silicates	0.50	Mn Oxides	0.33	Others	0.02	Monazite	0.02
Ilmenite	0.14	Ilmenite	0.33	Kaolinite	0.44	Kaolinite	0.31			Thorite	0.02
Spessartine	0.12	Kaolinite	0.26	Titanite	0.20	Calcite	0.23			Others	0
Chrome spinel	0.11	Spessartine	0.11	Ti-Magnetite	0.18	Ca-Fe-Al silicates	0.19				
Ti-Magnetite	0.05	Ti-Magnetite	0.08	Wolframite	0.03	Ilmenorutile	0.05				
Monazite	0.02	Monazite	0.04	Ilmenorutile	0.01	Others	0.22				
Ilmenorutile	0.01	Ilmenorutile	0.01	Spessartine	0.14						
Thorite	0.01	Columbite	0.01	Others	0.43						
Cu sulphides	0.01	Cu sulphides	0.01								
Others	0.89	Others	0.52								

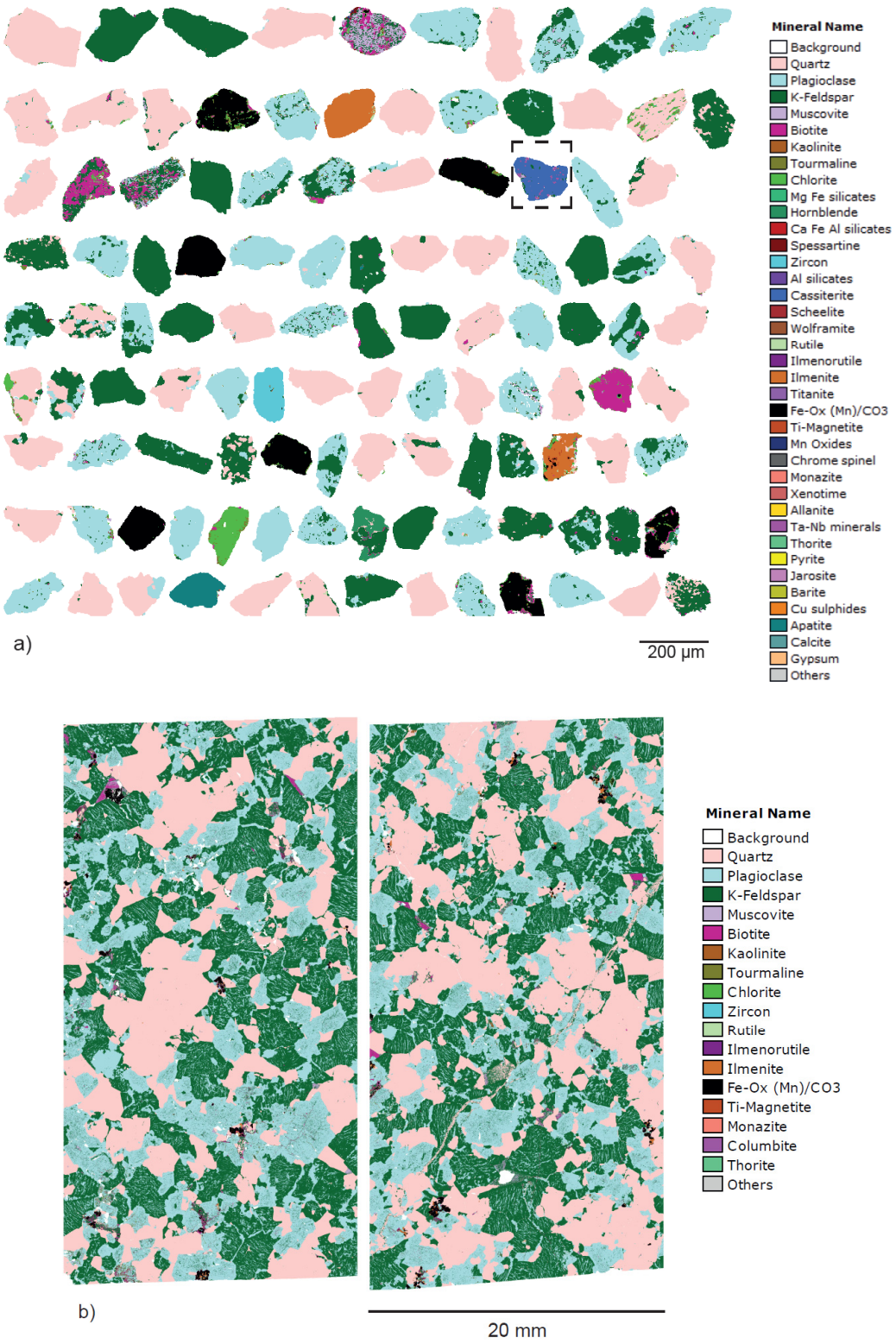

Figure 6. (**a**) Extract of studied composite QEMSCAN® mineral maps sorted by area and large to small particle size. The false colour image of the particles show their general mature appearance with a distinct lack of weathering rims and complete replacement. A cassiterite–columbite particle is indicated with a dashed rectangle and shown in Figure 7. (**b**) QEMSCAN® mineral maps of outcrop samples 17A (left) and 18A (right). Note the similarities in composition to composite mineral maps in a).

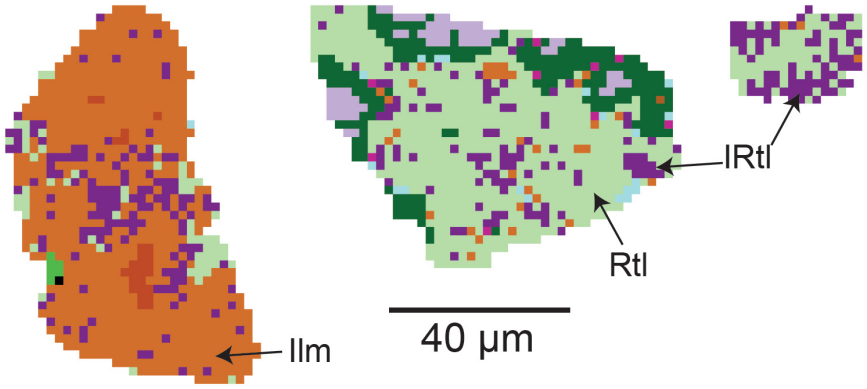

Figure 7. Stream sediment particles illustrating the intergrowth of rutile (rtl), ilmenorutile (irtl) and ilmenite (ilm). The legend is shown in Figure 6.

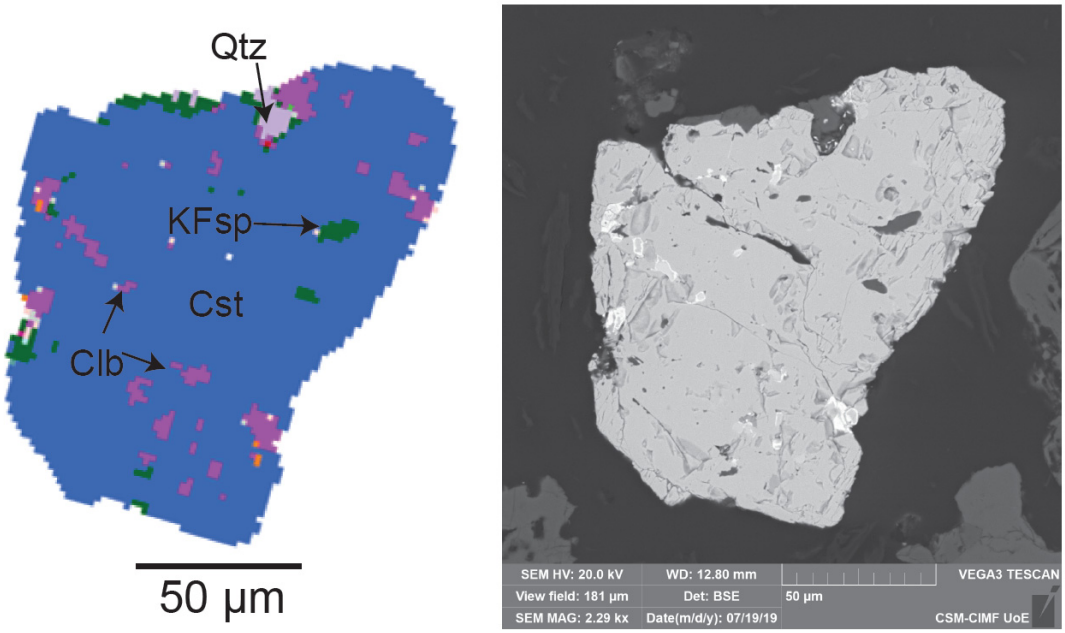

Figure 8. QEMSCAN® and SEM mineral map of a stream sediment particle (sample 16) showing the intergrowth of cassiterite (cst)–columbite (clb)–K–Feldspar (KFsp) and quartz (qtz).

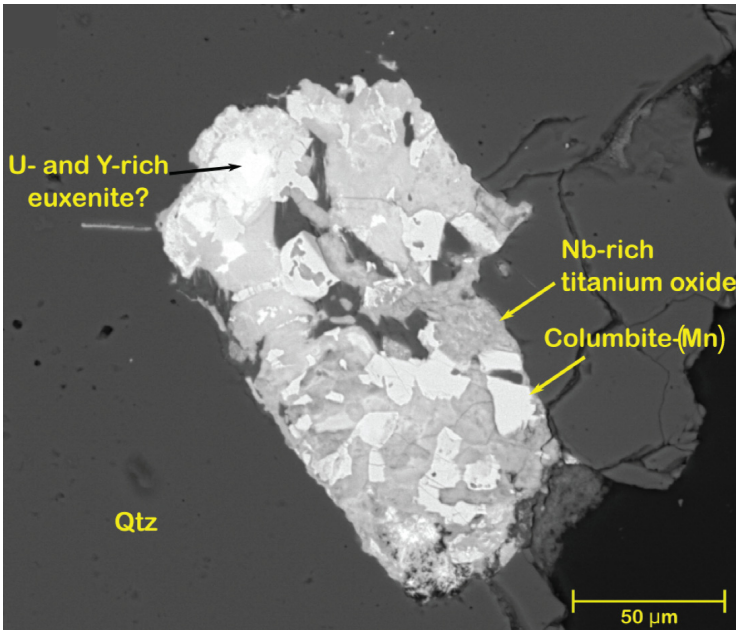

Figure 9. SEM image of stream sediment particle (sample 17) showing the intergrowth of Nb-rich titanium oxide (ilmenorutile), columbite (Mn) and euxenite (Y).

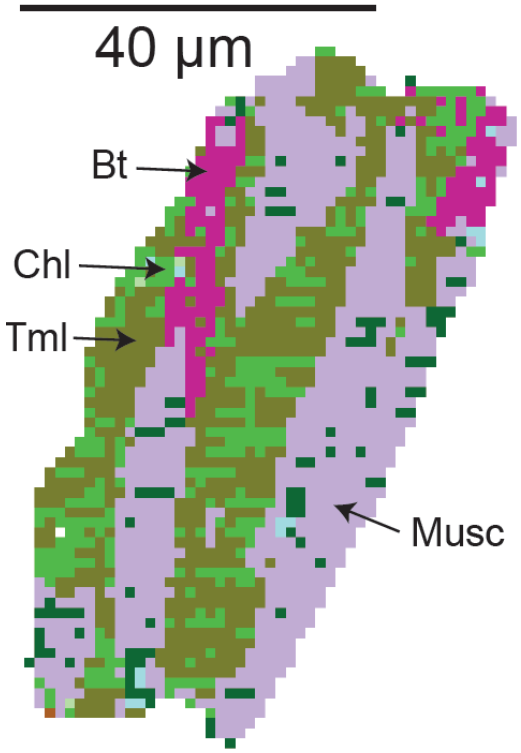

Figure 10. QEMSCAN® mineral map of stream sediment particle (sample 18) showing the intergrowth of chlorite (chl)–tourmaline (tml)–muscovite (musc)–biotite. This mineral association is interpreted to represent evidence for a granite-related magmatic–hydrothermal alteration.

5. Discussion

The graduated point symbol and bivariate fractionation plots demonstrate a distinctive endowment of base metals and high field strength elements (HFSE) in the northern Vosges magmatic suite, with a particular emphasis on the Natzwiller and Kagenfels Granite suites. The geochemical

trends observed in these plots are comparable with previous regional reconnaissance sampling [5] and whole-rock geochemical data presented in Tabaud et al. (2014) [6], particularly for Th, Sr, Rb and Ti, which provide a tool to distinguish intermediate and felsic magmatic rocks. The application of univariate anomaly mapping and the lithogeochemical classification of catchment sediments, therefore, supports the delineation of areas of increased enrichment of economically sought-after metals and corresponding magmatic lithologies. In particular, the present data confirm the known presence of Nb and Be and outline additional, previously unrecognised W anomalies in Kagenfels Granite.

Earlier empirical mineral and whole-rock geochemical studies have successfully demonstrated the use and application of magmatic fractionation ratios in defining late-stage magmatic melts prospective for Sn-W and Li-Cs-Ta mineralization [27,28,40–43]. Decreasing K/Rb, Nb/Ta, and Zr/Hf ratios indicate the increasing fractionation of the granitic melt and a transition to hydrothermal alteration [27]. Numerical changes in these ratios during late-stage magmatic fractionation are a result of the substitution of K with Rb in micas and feldspars [44], fractionation of Nb over Ta due to secondary muscovitisation and hydrothermal sub-solidus reactions enriching Ta in F-rich residual melts [29], and increasing Kd values of Hf in zircon, which are only weakly influenced by secondary fluid-related processes [28,45,46]. Recent geochemical studies of the Leinster Granite (Ireland) and Central Vosges Mg-K granites [3,30], along with mineralogical results of this study, have shown that these petrogenetic ratios are equally applicable to determine highly fractionated lithologies using geological materials affected by secondary dispersion processes, such as stream sediments. The lack of significant weathering of K, Rb, Sn, Nb and Zr-bearing silicate mineral phases in the analysed stream sediment fraction that were collected as well as the representativity of these stream sediments in relation to mapped and sampled outcrops of the catchment area confirm that these petrogenetic ratios can be employed to fingerprint fractionation patterns in the study area. In this context, the Natzwiller Granite shows fractionation ratios of $101 < K/Rb < 128.8$, $12.3 < Nb/Ta < 12.7$, and $33 < Zr/Hf < 36$ (Figure 3i–k), along with the generally highest Ti concentrations of 8640–10,500 ppm (Figure 5) evidenced by abundant rutile, ilmenite and titanite in the samples. Of particular interest are the elevated concentrations of incompatible elements, such as Li (105.1 ppm), W (34.81 ppm), Ta (8.1 ppm), B (21.99 ppm) and Be (13.47 ppm) in sample 2 along with abundant tourmaline (8.48%). In addition, despite a relatively low concentration of Sn (17.98 ppm) being measured in sample 20, automated mineralogical techniques identified multiple cassiterite grains in the stream sediment sample. This evidence suggests that the Natzwiller Granite has experienced, at least locally around NE–SW trending fault zones, the introduction of a highly fractionated melt enriched in fluxing elements, which allows incompatible and HFS elements to remain in late-stage, low-temperature melts [29]. Tabaud et al. (2014) [6] previously described the Natzwiller Granite as sub-aluminous to weakly peraluminous in nature, resulting from partial melting of an enriched mantle source and subsequent interaction with subducted metasedimentary and metaigneous crustal source material. Therefore, despite the comparably lower fractionation grade, the Natzwiller Granite was able to retain incompatible elements of possible economic interest.

In contrast, the peraluminous S-type Kagenfels Granite typically displays low values of $64.5 < K/Rb < 119$, $14 < Nb/Ta < 17.7$, and $19 < Zr/Hf < 38$ (Figure 3i–k), and therefore demonstrates a high degree of magmatic fractionation and secondary muscovitisation, characteristic of peraluminous S-type granites [27,42]. Geochemical fractionation trends (Figure 5), PC analysis (Figure 6) and mineralogical evidence in the form of tourmaline, muscovite, chlorite, wolframite, cassiterite, columbite and ilmenorutile imply a peraluminous evolution and confirm a highly fractionated and locally hydrothermally altered nature of the Kagenfels Granite. Strong fractionation of the melt, along with a predominant NE–SW structural control in the Kagenfels Granite, led to the emplacement of pegmatitic quartz-feldspar (-beryl) veins at "Grotte des Partisans" [23] and the Barembach stream confluences observed in the present study. The same process also resulted in characteristic elemental concentrations of As (25.52–92 ppm), Cu (7.88–166.61 ppm) and incompatible elements, such as Be (10–21 ppm), Sn (7.19–26.29 ppm), Li (12.13–52.61 ppm), and W (6.94–102.56 ppm). However, distinctive high values of $Nb/Ta > 17$ and the general absence of Li concentrations of >45 ppm across

the western part of the Kagenfels Granite (Figure 3h,j) suggest that, locally, magmatic fractionation and hydrothermal alteration processes were not as pronounced as in the eastern part of the Kagenfels Granite, which yields higher concentrations of Be (24–34.22 ppm), and Li (49.35–54.77 ppm), at 16.4 < Nb/Ta < 16.8, 64.5 < K/Rb < 93, and 19 < Zr/Hf < 25 (Figure 3h–k). The comparatively higher Nb/Ta ratios in the western Kagenfels Granite are a result of the predominant occurrence of Mn-columbite, euxenite-(Y), and Nb-rich titanium oxide/ ilmenorutile as evidenced in stream sediment sample 17 and 18. Consequently, the western part of the Kagenfels Granite predominantly produced a mineral assemblage with Nb > Ta-rich minerals, indicating the preferential fractionation of Nb over Ta-rich minerals and, therefore, the locally lower fractionation of the granitic melt. In a regional context, these observations imply that the Kagenfels Granite is the most fractionated granite suite in the northern Vosges Mountains, and consequently represents a prime target to explore for granite-hosted mineralisation.

The application of automated mineralogical techniques, such as QEMSCAN® and manual SEM-EDS, supported the routine collection of stream sediment samples in a mineral exploration context. These techniques were not only able to identify the bulk mineralogical composition of the stream sediment samples and therefore link geochemical signatures to source mineralogy, but also provide potential information about element deportment characteristics (ilmenorutile and columbite as principal Nb hosts, wolframite as principal W host, cassiterite as principal Sn host) for mineral processing-related studies. Therefore, this study, along with previous investigations into heavy mineral ilmenite deposits in India [8,9], demonstrates the usefulness of automated mineralogical techniques in early-stage exploration campaigns, which often predominantly involve the routine collection and analysis of stream sediment, soil and till samples and do not necessarily involve the link between sample geochemistry and mineralogical response and element deportment.

6. Conclusions and Implications for Mineral Exploration

This regional follow-up stream sediment exploration study has outlined geochemical and mineralogical evidence to support the previously established presence of Sn-W mineralization [5] and has provided new insights into this mineralisation suite, particularly regarding potential Li-Cs-Ta-Nb mineralisation in the S-type Kagenfels and I–S-type Natzwiller Granite suites of the northern Vosges Mountains. The occurrence of late-stage, incompatible elements in strongly fractionated lithologies and minerals implies the presence of a local mineralisation system. The Natzwiller and Kagenfels granites of the northern Vosges therefore warrant further exploratory work, particularly in areas of known structural control and occurrence of pegmatitic quartz–feldspar (-beryl) vein systems. The study has shown that automated mineralogical techniques can routinely be used in conjunction with univariate, multivariate and litho-geochemistry to determine the nature of stream sediments, source rock and generated exploration targets. A combined geochemical and mineralogical approach in early-stage grassroots exploration is therefore beneficial and useful when screening large areas during routine surveys.

Author Contributions: B.M.S. is the principal investigator on this project and compiled the data from fieldwork, geochemical and software analysis. B.M.S. also compiled the report. G.K.R. performed the QEMSCAN laboratory work and contributed to the methodology section of this paper. J.M.C. assisted in the fieldwork. **C**onceptualization, B.M.S.; methodology, B.M.S. and G.K.R.; software, B.M.S.; validation, B.M.S. and G.K.R.; formal analysis, B.M.S.; investigation, B.M.S.; resources, B.M.S.; data curation, B.M.S. and G.K.R.; writing—original draft preparation, B.M.S.; writing—review and editing, B.M.S.; visualization, B.M.S.; supervision, B.M.S.; project administration, B.M.S.; funding acquisition, B.M.S. and J.M.C.

Funding: The fieldwork was partly funded by a research grant from the McKinstry Fund of the Society of Economic Geologists Foundation Inc.

Acknowledgments: Sharon Uren and Stephen Pendray at Camborne School of Mines are thanked for providing assistance with the analytical work. Matthew Burford contributed to the field sampling in the Vosges.

Conflicts of Interest: The authors declare no conflict of interest.

Appendix A

Table A1. Modal mineralogy (mineral mass-%) of stream sediment and outcrop samples of the Kagenfels (14–19, yellow header) and Natzwiller Granites (2–3, 20, grey header).

Stream Sediment 2		Stream Sediment 3		Stream Sediment 14		Stream Sediment 15		Stream Sediment 16		Stream Sediment 17	
Plagioclase	27.08	Plagioclase	29.01	Plagioclase	35.30	Plagioclase	32.18	Plagioclase	32.38	Plagioclase	29.24
Quartz	19.6	K-Feldspar	20.96	K-Feldspar	28.96	K-Feldspar	25.12	K-Feldspar	26.44	Quartz	24.10
K-Feldspar	18.53	Quartz	19.65	Quartz	22.12	Quartz	24.30	Quartz	22.27	K-Feldspar	22.14
Chlorite	13.61	Chlorite	6.88	Fe-Ox (Mn)/CO3	4.58	Fe-Ox (Mn)/CO3	3.35	Fe-Ox (Mn)/CO3	6.98	Fe-Ox (Mn)/CO3	5.89
Tourmaline	8.48	Fe-Ox (Mn)/CO3	6.73	Chlorite	1.47	Chlorite	3.14	Zircon	2.27	Chlorite	3.52
Biotite	3.26	Hornblende	3.86	Biotite	1.26	Hornblende	2.17	Chlorite	2.10	Zircon	3.10
Fe-Ox (Mn)/CO3	2.07	Tourmaline	3.39	Zircon	1.20	Biotite	1.52	Biotite	1.48	Hornblende	3.03
Hornblende	1.92	Zircon	2.3	Ilmenite	0.98	Tourmaline	1.33	Hornblende	1.48	Biotite	2.01
Muscovite	1.12	Biotite	1.98	Muscovite	0.83	Zircon	1.20	Ilmenite	0.87	Tourmaline	1.43
Rutile	1.09	Apatite	1.26	Rutile	0.77	Rutile	1.10	Muscovite	0.80	Muscovite	1.34
Kaolinite	0.76	Rutile	1.11	Tourmaline	0.51	Muscovite	0.84	Tourmaline	0.74	Apatite	0.97
Zircon	0.57	Muscovite	0.71	Hornblende	0.49	Ca-Fe-Al silicates	0.43	Rutile	0.73	Rutile	0.70
Ca-Fe-Al silicates	0.38	Ca-Fe-Al silicates	0.42	Monazite	0.40	Kaolinite	0.40	Apatite	0.40	Ilmenite	0.60
Titanite	0.17	Titanite	0.37	Kaolinite	0.36	Ilmenite	0.28	Kaolinite	0.32	Ca-Fe-Al silicates	0.50
Ilmenite	0.14	Ilmenite	0.33	Spessartine	0.21	Thorite	0.21	Ca-Fe-Al silicates	0.17	Kaolinite	0.44
Spessartine	0.12	Kaolinite	0.26	Ca-Fe-Al silicates	0.17	Apatite	0.18	Ti-Magnetite	0.13	Titanite	0.20
Chrome spinel	0.11	Spessartine	0.11	Ilmenorutile	0.04	Spessartine	0.17	Spessartine	0.11	Ti-Magnetite	0.18
Ti-Magnetite	0.05	Ti-Magnetite	0.08	Others	0.35	Mn Oxides	0.10	Monazite	0.11	Wolframite	0.03
Monazite	0.02	Monazite	0.04			Columbite	0.01	Ilmenorutile	0.02	Ilmenorutile	0.01
Ilmenorutile	0.01	Ilmenorutile	0.01			Cu sulphides	0.01	Cassiterite	0.01	Spessartine	0.14
Thorite	0.01	Columbite	0.01			Ilmenorutile	0.01	Others	0.19	Others	0.43
Cu sulphides	0.01	Cu sulphides	0.01			Others	1.95				
Others	0.89	Others	0.52								

Stream Sediment 18		Rock 17A		Rock 18A		Stream Sediment 19		Stream Sediment 20	
Plagioclase	36.97	K-Feldspar	35.78	Quartz	36.55	Plagioclase	33.93	Plagioclase	31.05
K-Feldspar	25.9	Plagioclase	32.23	K-Feldspar	31.35	K-Feldspar	23.32	Quartz	24.65
Quartz	24.34	Quartz	29.44	Plagioclase	29.65	Quartz	29.01	K-Feldspar	22.23
Chlorite	2.56	Fe-Ox (Mn)/CO3	0.77	Fe-Ox (Mn)/CO3	0.8	Chlorite	2.88	Fe-Ox (Mn)/CO3	9.81
Fe-Ox (Mn)/CO3	1.91	Biotite	0.72	Biotite	0.53	Fe-Ox (Mn)/CO3	2.75	Chlorite	2.49
Biotite	1.79	Muscovite	0.46	Muscovite	0.42	Biotite	1.28	Biotite	1.82
Muscovite	1.37	Tourmaline	0.29	Tourmaline	0.22	Muscovite	1.46	Tourmaline	1.23
Ilmenite	0.91	Chlorite	0.12	Ilmenite	0.18	Tourmaline	0.92	Muscovite	1.16

Tourmaline	0.82	Ilmenite	0.09	Chlorite	0.12	Hornblende	0.75	Cassiterite	1.04
Spessartine	0.65	Rutile	0.04	Kaolinite	0.05	Ca-Fe-Al silicates	0.4	Zircon	0.93
Zircon	0.56	Zircon	0.02	Rutile	0.04	Spessartine	0.38	Calcite	0.93
Hornblende	0.48	Ti-Magnetite	0.01	Zircon	0.03	Zircon	0.54	Rutile	0.84
Rutile	0.41	Monazite	0.01	Ti-Magnetite	0.02	Rutile	0.62	Ilmenite	0.76
Mn Oxides	0.33	Others	0.02	Monazite	0.02	Ilmenorutile	0.01	Kaolinite	0.33
Kaolinite	0.31			Thorite	0.02	Ilmenite	0.59	Apatite	0.19
Calcite	0.23			Others	0	Titanite	0.13	Hornblende	0.14
Ca-Fe-Al silicates	0.19					Mn Oxides	0.2	Ti-Magnetite	0.12
Ilmenorutile	0.05					Columbite	0.01	Columbite	0.01
Others	0.22					Cu sulphides	0.01	Others	0.27
						Kaolinite	0.54		
						Others	0.27		

Table A2. Raw geochemical data for the present geochemical study. The stream sediment grain size fraction analysed was <75 μm. All 20 samples were analysed by ICP-MS using a four-acid digest (HCl-HF-HNO_3-$HClO_4$).

Sample ID	As (ppm)	B (ppm)	Be (ppm)	Cs (ppm)	Cu (ppm)	Hf (ppm)	K (ppm)	Li (ppm)	Nb (ppm)	Pb (ppm)	Rb (ppm)	Sn (ppm)	Sr (ppm)	Ta (ppm)	Th (ppm)	Ti (ppm)	W (ppm)	Zr (ppm)
1	15.35	60.25	6.35	14.41	375.63	10.11	12,513	64.24	31.12	54.29	110.2	18.4	214.44	2.54	23.37	4980	11.39	378.28
2	30.45	21.99	13.47	19.53	85.34	36.88	14,558	105.1	100.33	52.22	144.1	18.38	262.37	8.12	77.95	10,502.82	21.55	1248.59
3	18.67	15.41	10.2	12.65	86.53	50.3	18,186	81.56	94.64	33.29	141.2	13.66	291.31	7.45	93.73	8639.58	34.81	1833.39
4	9.38	15.38	2.33	10.63	51.75	22.96	19,889	51.79	15.16	36.07	142.3	19.48	138.48	1.39	14.99	4241.68	21.96	1033.49
5	13.69	15.26	2.82	16.5	49.65	19.83	15,368	66.7	14.62	77.18	114.5	13.28	177.75	1.82	15.89	5048.43	36.05	844.8
6	7.28	15.43	1.25	11.99	42.99	8.65	15,425	42.14	13.47	39.22	104.3	6.31	199.66	1.16	10.41	4723.44	49.9	346.08
7	16.41	14.31	3.68	17.92	62.55	9.61	16,553	78.27	15.28	93.69	116.4	5.48	132.92	1.85	10.07	5498.79	1.89	381.42
8	19.26	14.75	2.29	11.94	176.48	18.39	20,405	61.55	20.85	40.06	136.4	30.69	134.35	1.91	19.59	5539.26	6.92	776.97
9	50.27	13.48	1.73	27.42	70.08	12.41	18,473	79.66	9.93	28.29	77.9	34.06	98.89	0.76	8.87	4093.86	3.53	478.42
10	125.97	12.8	24.06	9.25	25.05	37.22	23,638	54.77	198.29	54.23	366.6	6.5	53.17	11.77	59.76	2170.97	11.83	711.86
11	73.95	13.85	34.22	10.88	48.77	32.66	18,266	49.35	126.27	46.11	195.5	30.82	49.41	7.55	66.3	2637.35	10.42	827.32
12	17.55	15.45	2.8	11.93	102.23	13.38	17,816	41.45	18.29	26.97	152.2	41.55	102.73	1.55	24.45	3839.98	1.8	552.45
13	44.09	12.1	10.32	3.59	7.88	35.85	22,682	12.13	99.06	8.72	190.2	7.19	21.41	5.87	47.58	2784.06	14.56	905.28
14	92.71	12.7	19.18	9.54	60.8	64.86	25,376	34.12	192.26	26.08	242	21.92	43.13	10.83	86.53	3994	8.76	1695.02
15	25.52	11.25	13.66	13.29	120.18	40.27	15,796	44.4	53.14	35.79	157	21.61	147.74	3.8	38.33	4208.34	29.11	1408.45
16	52.17	9.91	13.41	10.53	88.88	45.08	21,273	41.38	92.71	20.13	210.1	26.29	101.8	5.85	56.71	4133.23	28.7	1441.4
17	28.68	9.9	12.82	12.14	122.74	50.72	19,535	52.61	63.67	39.57	177.7	14.14	183.39	4.55	66.16	5683.34	102.56	1923.08
18	83.4	10.46	21.8	7.62	59.56	34.05	20,270	26.16	92.76	26.64	186.4	10.07	36.22	5.5	46.62	3223.2	6.94	899.06
19	68.71	12.02	10.22	11.36	166.61	28.35	15,251	35.5	66.55	40.69	152.7	20.05	78.5	4.06	41.08	3681.99	10.84	870.06
20	9.04	15.46	8.03	9.35	116.28	17.45	12,924	47.29	29.72	99.56	47.3	17.98	179.99	2.69	21.65	3896.3	23.26	698.02

References

1. European Commission. *Directorate-General for Internal Market, Industry, Entrepreneurship and SMEs (European Commission) Study on the Review of the List of Critical Raw Materials 2017*; European Commission: Brussels, Belgium, 2017.
2. Romer, R.L.; Kroner, U. Phanerozoic tin and tungsten mineralization—Tectonic controls on the distribution of enriched protoliths and heat sources for crustal melting. *Gondwana Res.* **2016**, *31*, 60–95.
3. Steiner, B.M. W and Li-Cs-Ta signatures in I-type granites—A case study from the Vosges Mountains, NE France. *J. Geochem. Expl.* **2019**, *197*, 238–250.
4. Bureau de Recherches Géologiques et Minières BRGM InfoTerre. Available online: http://www.infoterre.brgm.fr (accessed on 20 October 2019).
5. Leduc, C. *Paris-Vosges—Zones D et E. Prospection Géochimique Stratégique Cirey-sur-Vezouze et Molsheim. Interprétation des Résultats Analytiques*; Bureau de Recherches Géologiques et Minières: Orléans, France, 1984; p. 93.
6. Tabaud, A.-S.; Whitechurch, H.; Rossi, P.; Schulmann, K.; Guerrot, C.; Cocherie, A. Devonian–Permian magmatic pulses in the northern Vosges Mountains (NE France): Result of continuous subduction of the Rhenohercynian Ocean and Avalonian passive margin. *Geol. Soc. Lond.* **2014**, *405*, 197–223.
7. Altherr, R.; Holl, A.; Hegner, E.; Langer, C.; Kreuzner, H. High-potassium, calc-alkaline I-type plutonism in the European Variscides: Northern Vosges (France) and northern Schwarzwald (Germany). *Lithos* **2000**, *50*, 51–73.
8. Bernstein, S.; Frei, D.; McLimans, R.K.; Knudsen, C.; Vasudev, V.N. Application of CCSEM to heavy mineral deposits: Source of high-Ti ilmenite sand deposits of South Kerala beaches, SW India. *J. Geochem. Expl.* **2008**, *96*, 25–42.
9. Keulen, N.; Frei, D.; Riisager, P.; Knudsen, C. Analysis of heavy minerals in sediments by computer-controlled scanning electron microscopy (CCSEM): Principles and applications. *Mineral. Assoc. Can. Short Course* **2012**, *42*, 67–184.
10. Mackay, D.A.R.; Simandl, G.J.; Ma, W.; Redfearn, M.; Gravel, J. Indicator mineral-based exploration for carbonatites and related specialty metal deposits—A QEMSCAN® orientation survey, British Columbia, Canada. *J. Geochem. Expl.* **2016**, *165*, 159–173.
11. Piqué, A.; Fluck, P.; Schneider, J.L.; Whitechurch, H. The Vosges Massif. In *Pre-Mesozoic Geology in France and Related Areas*; Chantraine, J., Rolet, J., Santallier, D.S., Piqué, A., Keppie, J.D., Eds.; IGCP-Project 233; Springer: Berlin, Heidelberg, 1994; pp. 416–425.
12. Tabaud, A.-S.; Janoušek, V.; Skrzypek, E.; Schulmann, K.; Rossi, P.; Whitechurch, H.; Guerrot, C.; Paquette, J.-L. Chronology, petrogenesis and heat sources for successive Carboniferous magmatic events in the Southern–Central Variscan Vosges Mts (NE France). *J. Geol. Soc.* **2015**, *172*, 87–102.
13. Schulmann, K.; Martínez Catalán, J.R.; Lardeaux, J.M.; Janoušek, V.; Oggiano, G. The Variscan orogeny: Extent, timescale and the formation of the European crust. *Geol. Soc. Lond.* **2014**, *405*, 1–6.
14. Hess, J.C.; Lippolt, H.J.; Kober, B. The age of the Kagenfels granite (northern Vosges) and its bearing on the intrusion scheme of late Variscan granitoids. *Geol. Rundsch.* **1995**, *84*, 568–577.
15. Elsass, P.; Eller, J.P.; Stussi, J.M. *Géologie du Massif du Champ du Feu et de ses Abords: Éléments de Notice Pour la Feuille Géologique 307 Sélestat.*; Bureau de Recherches Géologiques et Minières: Orléans, France, 2008; p. 187.
16. Dekoninck, A.; Rochez, G.; Yans, J.; Fluck, P. Mineralizing events in the Vosges massif: Insights from the Mn-W Haut-Poirot deposit (NE France). *Proc. Miner. Resour. Discov.* **2017**, *4*, 1519–1522.
17. Fluck, P.; Stein, S. Espèces minérales des principaux districts miniers du massif vosgien. *Pierres et Terre* **1992**, *35*, 107–115.
18. Fluck, P. *Metallogeny of Vosges*; Freiberger Forschungshefte: Salamanca, Spain, 1977; pp. 83–93.
19. Fluck, P.; Weil, R. *Géologie des Gîtes Minéraux des Vosges et des Régions Limitrophes*; Mémoires du, B.R.G.M. Ed.; Bureau de Recherches Géologiques et Minières: Orléans, France, 1976.
20. Mariet, A.L.; Bégeot, C.; Gimbert, F.; Gauthier, J.; Fluck, P.; Walter-Simonnet, A.V. Past mining activities in the Vosges Mountains (eastern France): Impact on vegetation and metal contamination over the past millennium. *Holocene* **2016**, *26*, 1225–1236.

21. Forel, B.; Monna, F.; Petit, C.; Bruguier, O.; Losno, R.; Fluck, P.; Begeot, C.; Richard, H.; Bichet, V.; Chateau, C. Historical mining and smelting in the Vosges Mountains (France) recorded in two ombrotrophic peat bogs. *J. Geochem. Expl.* **2010**, *107*, 9–20.
22. Billa, M.; Gloaguen, E.; Melleton, J.; Tourlière, B. *Consolidation des Anomalies Géochimiques et Géophysiques du Territoire Métropolitain*; Bureau de Recherches Géologiques et Minières: Orléans, France, 2016; p. 42.
23. Weil, R. Sur la présence de l'adulaire dans la Grotte des Partisans. *Sciences Géologiques Bulletins et Mémoires* **1936**, *3*, 27–28.
24. Bureau de Recherches Géologiques et Minières SIG Mines France. Available online: http://sigminesfrance.brgm.fr/sig.asp (accessed on 20 October 2019).
25. Schneider, M. *Vogesengranit—Letter: Natzweiler-Struthof Memorial Museum Collection 1940*, Natzweiler-Struthof Memorial Museum Collection: Natzwiller, France, 1940.
26. Steiner, B.M. Tools and Workflows for Grassroots Li-Cs-Ta (LCT) pegmatite exploration. *Minerals* **2019**, *9*, 499–522.
27. Ballouard, C.; Poujol, M.; Boulvais, P.; Branquet, Y.; Tartèse, R.; Vigneresse, J.L. Nb-Ta fractionation in peraluminous granites: A marker of the magmatic–hydrothermal transition. *Geology* **2016**, *44*, 231–234.
28. Breiter, K.; Škoda, R. Zircon and whole-rock Zr/Hf ratios as markers of the evolution of granitic magmas: Examples from the Teplice caldera (Czech Republic/Germany). *Mineral. Petrol.* **2017**, *111*, 435–457.
29. Linnen, R.L.; Keppler, H. Columbite solubility in granitic melts: Consequences for the enrichment and fractionation of Nb and Ta in the Earth's crust. *Contrib. Mineral. Petrol.* **1997**, *128*, 213–227.
30. Steiner, B.M. Using Tellus stream sediment geochemistry to fingerprint regional geology and mineralisation systems in southeast Ireland. *Irish J. Earth Sci.* **2018**, *36*, 45–61.
31. Gottlieb, P.; Wilkie, G.; Sutherland, D.; Ho-Tun, E.; Suthers, S.; Perera, K.; Jenkins, B.; Spencer, S.; Butcher, A.; Rayner, J. Using Quantitative Electron Microscopy for Process Mineralogy Applications. *Jom* **2000**, *52*, 24–25.
32. Pirrie, D.; Butcher, A.; Power, M.R.; Gottlieb, P.; Miller, G.L. Rapid quantitative mineral and phase analysis using automated scanning electron microscopy (QEMSCAN®); potential applications in forensic geoscience. *Geol. Soc. Lond.* **2004**, *232*, 123–136.
33. Pirrie, D.; Rollinson, G.K. Unlocking the applications of automated mineral analysis. *Geol. Today* **2011**, *27*, 235–244.
34. Rollinson, G.K. Automated Mineralogy by SEM-EDS. In *Earth Systems and Environmental Sciences*; Science Direct; John Wiley and Sons: Hoboken, NJ, USA, 1996.
35. Rollinson, G.K.; Stickland, R.J.; Andersen, J.C.Ø.; Fairhurst, R.; Boni, M. Characterisation of Supergene Non-Sulphide Zinc Deposits using QEMSCAN®. *Miner. Eng.* **2011**, *24*, 778–787.
36. Simons, B.; Rollinson, G.K.; Andersen, J.C.Ø. Characterisation of lithium minerals in granite-related pegmatites and greisens by SEM-based automated mineralogy 2018. In Proceedings of the Mineral Deposits Study Group Winter Meeting, Brighton, UK, 3–5 January, 2018.
37. Taylor, S.R. Abundance of chemical elements in the continental crust: A new table. *Geochim. Cosmochim. Acta* **1965**, *28*, 1273–1285.
38. Andersen, J.C.Ø.; Stickland, R.J.; Rollinson, G.K.; Shail, R.K. Indium mineralisation in SW England: Host parageneses and mineralogical relations. *Ore Geol. Rev.* **2016**, *78*, 213–238.
39. Fleet, M.E. *Sheet Silicates: Micas*; Deer, Howie and Zussman Rock Forming Minerals Series; Geological Society: London, UK, 2003.
40. Breiter, K.; Ďurišová, J.; Hrstka, T.; Korbelová, Z.; Vašinová Galiová, M.; Müller, A.; Simons, B.; Shail, R.K.; Williamson, B.J.; Davies, J.A. The transition from granite to banded aplite-pegmatite sheet complexes: An example from Megiliggar Rocks, Tregonning topaz granite, Cornwall. *Lithos* **2018**, *302*, 370–388.
41. Simons, B.; Andersen, J.C.Ø.; Shail, R.K.; Jenner, F.E. Fractionation of Li, Be, Ga, Nb, Ta, In, Sn, Sb, W and Bi in the peraluminous Early Permian Variscan granites of the Cornubian Batholith: Precursor processes to magmatic-hydrothermal mineralisation. *Lithos* **2017**, *278*, 491–512.
42. Selway, J.B.; Breaks, F.W.; Tindle, A.G. Pegmatite Exploration Techniques for the Superior Province, Canada, and Large Worldwide Tantalum Deposits. *Explor. Min. Geol.* **2005**, *14*, 1–30.
43. Černý, P. Exploration strategy and methods for pegmatite deposits of tantalum. In *Lanthanides, Tantalum, and Niobium*; Moller, P., Černý, P., Saupe, F., Eds.; Springer: New York, NY, USA, 1989; pp. 274–302.
44. Shaw, D. A review of K-Rb fractionation trends by covariance analysis. *Geochim. Cosmochim. Acta* **1968**, *32*, 573–601.

45. Bau, M. Controls on the fractionation of isovalent trace elements in magmatic and aqueous systems: Evidence from Y/Ho, Zr/Hf, and lanthanide tetrad effect. *Contrib. Mineral. Petrol.* **1996**, *123*, 323–333.
46. Fujimaki, H. Partition-coefficients of Hf, Zr, and REE between zircon, apatite and liquid. *Contrib. Mineral. Petrol.* **1986**, *94*, 42–45.